Mesoscale Correlation Length Scales from NSCAT and Minimet Surface Wind Retrievals in the Labrador Sea

R. F. MILLIFF

Colorado Research Associates, NorthWest Research Associates, Boulder, Colorado

P. P. NIILER

Scripps Institution of Oceanography, La Jolla, California

J. MORZEL

Colorado Research Associates, Boulder, Colorado

A. E. SYBRANDY

Pacific Gyre Corporation, Carlsbad, California

D. NYCHKA AND W. G. LARGE

National Center for Atmospheric Research, Boulder, Colorado

(Manuscript received 29 November 2001, in final form 1 August 2002)

ABSTRACT

Observations of the surface wind speed and direction in the Labrador Sea for the period October 1996–May 1997 were obtained by the NASA scatterometer (NSCAT), and by 21 newly developed Minimet drifting buoys. Minimet wind speeds are inferred, hourly, from observations of acoustic pressure in the Wind-Speed Observation Through Ambient Noise (WOTAN) technology. Wind directions are inferred from a direction histogram, also accumulated hourly, as determined by the orientation of a wind vane attached to the surface floatation. Effective temporal averaging of acoustic pressure (20 min), and the interval over which the direction histogram is accumulated (160 s), are shown to be consistent with low-pass filtering to preserve mesoscale time- and space-scale signals in the surface wind. Minimet wind speed and direction retrievals in the Labrador Sea were calibrated with collocated NSCAT data. The NSCAT calibrations extend over the full field lifetimes of each Minimet (90 days on average). Wind speed variabilities of $O(5\ \mathrm{m\ s^{-1}})$ and wind direction variabilities of $O(40^\circ)$ are evident on timescales of one to several hours in Minimet time series. Wind speed and direction rms differences versus spatial separation comparisons (from 0 to 400 km) for the NSCAT and Minimet records demonstrate similar rms differences in wind speed as a function of spatial separation, but $O(20^\circ)$ larger rms differences in Minimet direction. These differences are consistent with spatial smoothing effects in the median filter step for wind direction retrievals within the NSCAT swath. Zonal and meridional surface wind components are constructed from the calibrated Minimet wind speed and direction dataset. Rms differences versus spatial separation for these components are used to estimate mesoscale spatial correlation length scales of 250 and 290 km in the zonal and meridional directions, respectively.

1. Introduction

The purposes of this paper are twofold: first, to introduce the surface wind observation capabilities of Minimet drifter systems as demonstrated in their first deployments in the Labrador Sea; and second, to demonstrate how Minimet observations, in concert with coincident scatterometer data, can recover spatial properties of the mesoscale marine surface wind field.

Nested levels of organization are often defined to characterize geophysical fluid motions in terms of pairings of time- and space scales that are observed to occur in natural systems. The wind field at the surface of the ocean is amenable to characterizations of this kind. Three levels of organization of the surface wind field are relevant to this study; namely, the microscale, the mesoscale, and the synoptic scale.

Synoptic-scale features of the surface wind field in

Corresponding author address: Dr. Ralph F. Milliff, Colorado Research Associates, 3380 Mitchell Ln, Boulder, CO 80301-5410.
E-mail: miliff@coloradoresearch.com

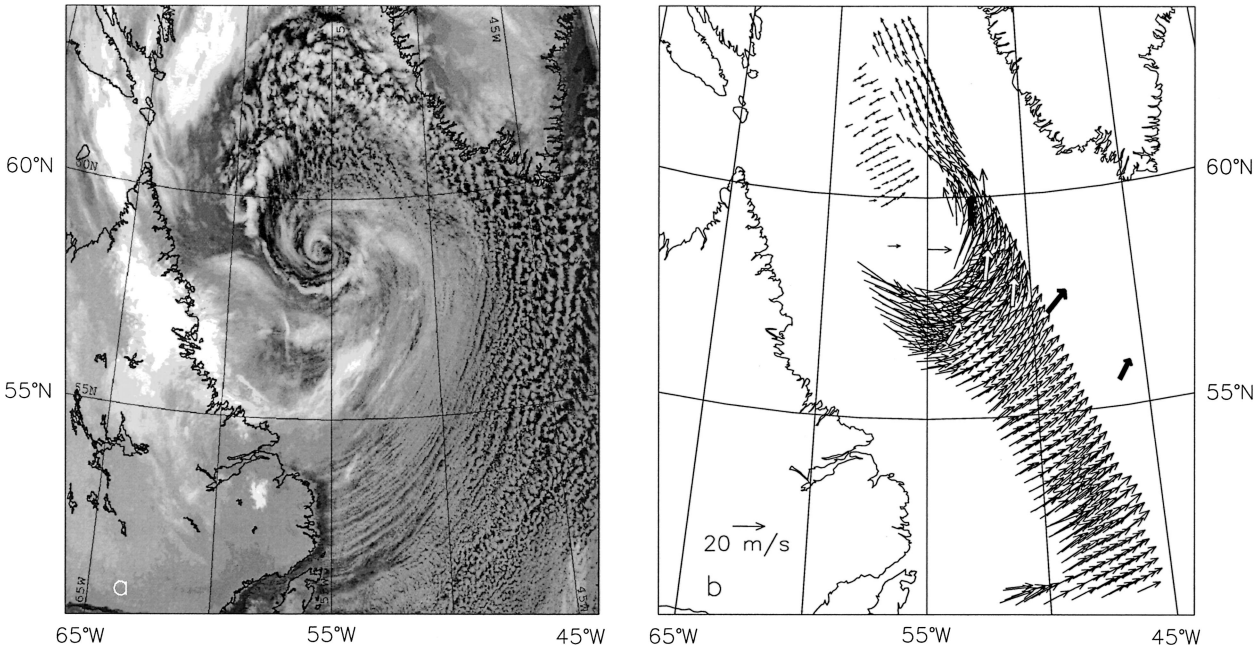

FIG. 1. Satellite and drifter observations in the Labrador Sea. (a) AVHRR infrared satellite image of the Labrador Sea region from *NOAA-12* at 2103 UTC 30 Jan 1997. Cold cloud tops and ice surfaces appear in lighter shades, while the relatively warm sea surface is dark. The coastlines for Labrador in the southwest and Greenland in the northeast are overlaid in black [image adapted from Renfrew et al. (1999); used with permission]. (b) NSCAT wind vectors at 0052 UTC 31 Jan 1997 (revolution no. 2382) from the Ku2000 GMF retrievals with six Minimet observations from within 18–53 min of the satellite image. Solid arrows are Minimet drifter data with observed wind directions and speeds, and open arrows are observed Minimet drifter directions and nearest-neighbor NSCAT speeds. Rain-flagged retrievals in the NSCAT surface wind vectors have been removed from the snapshot in (b). Nonetheless, vector wind retrievals north of 60°N, and between 55° and 60°W, exhibit rain-contaminated behaviors such as cross-swath orientation and discontinuities in the implied flow field that do not make meteorological sense.

the Labrador Sea region occur on timescales from hours to days and spatial scales that span the subbasin. An example is the basin-scale low pressure system circulations evident in the radiances from the Advanced Very High Resolution Radiometer (AVHRR) image in Fig. 1a. This particular image captures a deep low pressure system that occupied the Labrador Sea region on 30 January 1997 at 2103 UTC [image adapted from Renfrew et al. (1999)]. Cold cloud tops, ice, and land surfaces appear in the image as lighter shades, while the relatively warm sea surface is dark. Intense low pressure systems of the kind depicted in Fig. 1 typically form and propagate eastward across the Labrador Sea in about a day. They provide the atmospheric forcing to precondition for—and later in the season, to trigger—ocean deep convection processes that have been observed in the Labrador Sea in winter (e.g., Lab Sea Group 1998). A comprehensive description and simulation of so-called polar low formation and propagation in the Labrador Sea is provided by Pagowski and Moore (2001).[1]

Mesoscale fluctuations in the surface wind field occur on timescales from one to tens of hours (e.g., Pierson 1983; Austin and Pierson 1999), and on spatial scales from tens to hundreds of kilometers. The mesoscale variability often occurs as intermittent and organized fluctuations within identifiable regimes of the synoptic-scale patterns. For example, in Fig. 1, the surface pressure minimum occurs at about 58°N, 55°W at the center of a characteristic spiral cloud formation. In a mesoscale regime to the southeast, cloud streaks align in the direction of a vigorous wind oriented directly offshore near the southern extreme of the Labrador coastline, veering toward the low over the basin. These cloud formations are indicators of energetic roll vortices (roll circulation orthogonal to the surface wind direction; Renfrew and Moore 1999) that are implicated in massive heat and moisture fluxes from the sea surface. In another mesoscale regime to the northeast of the surface pressure minimum, the cloud patterns are indicative of atmospheric convection in more cellular structures.

The atmospheric microscale is characterized by timescales from seconds to 1 h, and spatial scales from 1 to 10 km. As such, microscale signals are not evident in Fig. 1. Planetary effects are not important on these scales, and strong connections to isotropic turbulence theory and laboratory experiments can be made. Through an approximation often called a Taylor hy-

[1] Pagowski and Moore (2001) refer to polar lows as synoptic systems, but to distinguish polar lows from more common low pressure systems in middle latitudes they also use the term ''mesocyclone.'' This is not to be confused with what we are referring to as mesoscale in the present paper.

pothesis microscale fluctuations in time can be interpreted to imply microscale spatial dimensions, and vice versa (e.g., Lumley and Panofsky 1964). That is $Tu \approx L$, where T is the period, u is a characteristic microscale velocity, and L is a microscale length scale. Spectral properties of the microscale surface layer wind are quantified and generalized in Kaimal et al. (1972). While these properties derive from measurements over land, the authors demonstrate that the normalized spectra from over-water field experiments exhibit similar behaviors. Importantly, Kaimal et al. (1972) demonstrate a peak in surface velocity spectra (longitudinal and transverse components), occurring at higher frequencies quite apart from the energy at mesoscale frequencies. This gives rise to the widespread notion of a *spectral gap* between the microscale and mesoscale energy in the surface wind field.

Surface wind observing systems can be placed in the context of these levels of organization. In this paper we will describe averaging of samples at microscale frequencies in Minimet drifters over timescales coincident with the spectral gap, as a means of low-pass filtering to isolate the mesoscale. Also, we will describe calibrations of Minimet wind speed and direction retrievals with near-neighbor NSCAT retrievals. We will show that these calibrations were necessary to extract geophysical information from the Minimet wind observations and set the mesoscale signal from Minimet data in its proper synoptic context.

The advent of calibrated satellite scatterometers has made possible continuous observation of synoptic patterns of the surface vector wind over large regions of World Ocean [see Jones et al. (1982) for a Seasat example; see also the National Aeronautics and Space Administration (NASA) scatterometer (NSCAT) papers following O'Brien (1999)]. Following the launch of the NSCAT instrument aboard the *ADEOS-I* satellite platform in August 1996, comparisons and calibrations were made using a variety of wind retrieval algorithms with in situ surface wind observations from moored buoys (e.g., Dickinson et al. 2001; Freilich and Dunbar 1999), research ships (Bourassa et al. 1997), and numerical weather prediction products (Liu et al. 1998; Atlas et al. 1999). These comparisons and calibrations, and the derivation of so-called geophysical model functions (GMFs) to retrieve vector wind information from radar backscatter, all focus on accurate reproduction of synoptic-scale surface winds. While the within-swath resolution for NSCAT is sufficient to resolve mesoscale spatial variability, it is the synoptic scales that are most apparent in the wind retrievals. Figure 1b demonstrates the surface wind retrievals from NSCAT within 4 h of the AVHRR image (Fig. 1a). The synoptic-scale circulation is consistent with the polar low that fills the Labrador Sea subbasin.

The spatial properties of the mesoscale surface wind variability over the ocean are very difficult to observe over spatial scales that approach the synoptic systems within which the mesoscale is embedded. A single polar-orbiting spaceborne system is incapable of achieving mesoscale temporal resolution uniformly over the globe (Milliff et al. 2001; Schlax et al. 2001). Spatial information regarding the mesoscale surface wind cannot be directly obtained from operational moored buoys [e.g., Tropical Atmosphere Ocean (TAO), National Data Buoy Center, etc.] as these are not deployed in mesoscale arrays. Neither can available ship observations be used since research vessel observations generally occur along straight cruise tracks, often on timescales longer than mesoscale. Weller et al. (1983) report that intercalibration issues for a mesoscale array of in situ surface wind sensors precluded detection of spatial properties of the mesoscale wind field during the Joint Air–Sea Interaction (JASIN) experiment.

In this paper we introduce the Minimet wind observing system. We show that using scatterometer wind observations, the Minimet dataset can be calibrated to provide first estimates of the spatial length scales of the mesoscale surface wind field for the Labrador Sea in winter. The NSCAT system and data for our study period are reviewed in section 2. The Minimet design and observing system heritage are introduced in section 3. Also in section 3, we review field calibrations and sample data from the Minimet wind observing systems deployed in the Labrador Sea. More detailed information concerning Minimet drifter design, data processing, and predeployment calibrations are provided in an appendix. In section 4 we compare the Labrador Sea Minimet winds with coincident NSCAT wind retrievals to demonstrate a mesoscale signal in the wintertime surface winds that is largely removed by NSCAT retrieval algorithms. First estimates of the spatial properties of the mesoscale surface wind field on the Labrador Sea in winter are derived to conclude this paper.

2. NSCAT wind retrievals in the Labrador Sea

The NSCAT mission from 15 September 1996 through 29 June 1997 spans the winter season of our study. A complete overview of the NSCAT instrument and mission is available from Naderi et al. (1991). NSCAT was a fan beam scatterometer that illuminated the sea surface with radar energy at a frequency of 14 GHz. Backscatter signals were detected from a variety of incidence and azimuth angles, and for horizontal and vertical radar polarizations, along three antennas (fore, mid, and aft beams) on each side of the NSCAT instrument. The incidence angle, azimuth angle, and polarization diversity accounted for complicated patterns of overlapping radar footprints at the surface [see Fig. 1 in Jones et al. (1999)]. These returns are composited over wind vector cell (WVC) areas of 25 km $\times$ 25 km. The composite backscatter from each WVC is related to a wind vector by inverting a GMF that relates the normalized radar backscatter to wind speed and wind direction, as well as other radar and geometric param-

eters. The radar backscatter in the NSCAT frequency range can be affected by heavy rain. Raindrops attenuate and backscatter the radar signal, as well as change the roughness of the sea surface. Wind vectors are retrieved for each WVC over the ice-free ocean and where the radar backscatter is not contaminated by rain. Globally, NSCAT sampled about 90% of the ice-free global ocean every 2 days.

Because of inherent measurement noise, typical GMF inversions yield several possible, or ambiguous, vector winds for a given WVC. Each ambiguity is assigned a likelihood in the GMF inversion algorithm. The range of wind speed ambiguities is found to be small, but the range of wind direction ambiguities can be large, with a significant number of direction ambiguities differing by 180°; the so-called upwind/downwind ambiguity. A median filter method (Shultz 1990; Shaffer et al. 1991; Gonzales and Long 1999) is used to iteratively select among ambiguities by finding the closest vector to the median of selected vectors in several neighboring WVCs. The iterative process is often initiated by finding the direction ambiguities closest to coarse-resolution weather center analyses [so-called numerical weather prediction (NWP) nudging].

The development and testing of geophysical model functions, including the median filter step, for scatterometer systems is an area of ongoing research (Wentz et al. 1984, 1986; Freilich and Challenor 1994; Freilich and Dunbar 1993a,b; Stoffelen and Anderson 1997; Gonzales and Long 1999; Mejia et al. 1999; Wentz and Smith 1999; Brown 2000). In our analyses, we have used the wind vector retrievals based on the NSCAT–Ku2000 GMF developed by Wentz and Smith (1999) (available online at Remote Sensing Systems at ftp://ftp.ssmi.com). Only the highest quality retrievals have been used, which exclude data identified as rain contaminated as well as retrievals with poor GMF fits. The NSCAT–Ku2000 retrievals correct for small global directional biases identified in prior retrieval products.[2] Wentz and Smith (1999) validate the NSCAT–Ku2000 wind speed and direction retrievals in comparisons with observations from moored ocean buoys, and with ocean surface wind analyses from the National Centers for Environmental Prediction. Average speed biases were within 1 m s^{-1} with an rms of 2 m s^{-1}. Wind direction biases are within 10° of the validation data, with an rms direction variability of 20°.

NSCAT coverage at latitudes 50°–65°N, in the Labrador Sea region, was excellent. NSCAT orbited the earth about 14 times per day, with exact repeat orbits every 41 days (NASA Scatterometer Project 1998). The NSCAT swath spans 600 km on either side of the subsatellite ground track, separated by a 400-km gap in coverage centered at nadir. Each swath is partitioned into 25 km × 25 km WVC; that is, 48 WVC in the cross-track direction. The NSCAT overflights of the Labrador Sea occurred near 0000 UTC (ascending orbital tracks) and 1400 UTC (descending orbital tracks). The Labrador Sea orientation is such that swath coverage spans the entire basin for a large subset of the ascending orbits in the region. Frequently, successive descending orbits overlap in the Labrador Sea region such that dense sampling of the surface wind field occurs within a 101-min time window (an example is depicted in Fig. 6, which will be discussed below).

To the extent that neighboring WVC wind directions influence the local wind direction ambiguity selection, the median filter operates as a spatial smoother on wind direction variability within the NSCAT swath. Since the wind speed ambiguities for each WVC do not differ widely, the spatial smoothing effect on speed is less pronounced. Thus, the 25-km WVC spacing within the NSCAT swath might be sufficient to resolve mesoscale spatial variability in wind speed, but spatial resolution of wind direction variability within the NSCAT swath is coarsened by the median filter. We will quantify these issues by comparison with Minimet drifter spatial resolutions for wind speed and direction in section 4.

3. Minimet observations of the surface wind field in the Labrador Sea

Design considerations in the development of surface wind observation systems for the Labrador Sea Minimet drifter deployments were driven in part by the goals of the Deep Convection Experiment as described by the Lab Sea Group (1998). The Minimet drifter wind observation systems were designed to be capable of reliable observations and remote communications for an entire winter season. Surface wind speed, wind direction, and ancillary data were obtained at mesoscale resolution under sustained conditions of very high winds and rough seas. The Labrador Sea Minimet drifter prototypes integrate advanced technologies that existed separately in drifter mechanical and electronic components, and in moored wind observing systems and compass technologies. Integrating these technologies in multiple durable Lagrangian packages for simultaneous deployments posed new challenges in data processing and remote communications as well. In this section we focus on the field calibrations and surface wind datasets to emerge from the Labrador Sea deployment. The upper-ocean response part of the Labrador Sea Minimet deployments will be described elsewhere. At several points in the discussion, the interested reader is referred to an appendix that details aspects of the Minimet wind observation system design and engineering calibrations that are critical to the introduction of this new instrument technology.

[2] The wind direction distribution function for NSCAT wind retrievals over the entire globe, based on the NSCAT-2 GMF from the NASA Jet Propulsion Laboratory, contained small artifacts associated with the antenna orientations. These were corrected in the NSCAT–Ku2000 GMF, which came later. The results of our study are not sensitive to these small effects.

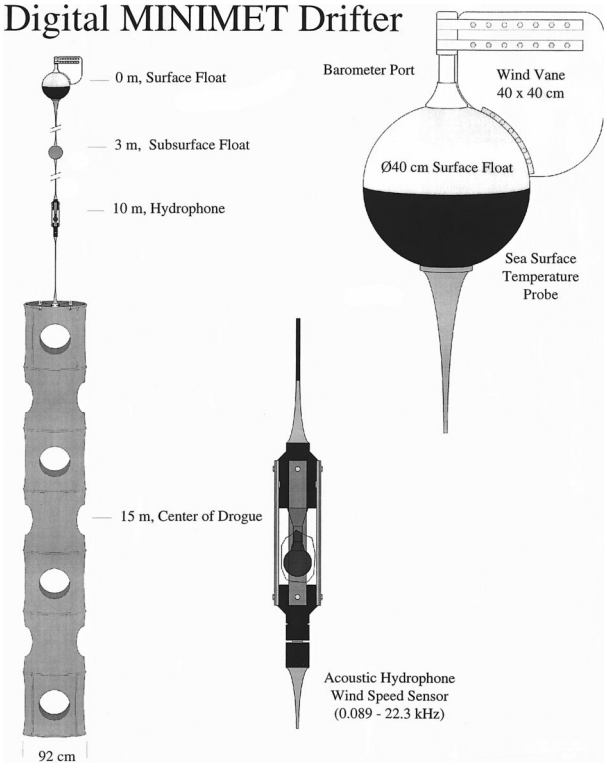

FIG. 2. Minimet drifter configuration. Schematics depicting the fully deployed Minimet drifter configuration including surface and subsurface floatation, the hydrophone cage, and a holey-sock drogue; an expanded view of the WOTAN instrument configuration; and an expanded diagram of the surface floatation components.

We will show that spatial properties of the surface mesoscale wind field are accessible from multiple [e.g., $O(10)$] in situ drifting Minimets that coincide with $O(100)$ NSCAT overflights of the study region. Deploying multiple in situ systems constrains costs such that construction, deployment, and calibration procedures for each drifter must be inexpensive and repeatable. For example, drifter recovery and individual postcalibrations are not practical. Requiring long field lifetimes [e.g., $O(100$ days$)$] for each drifter constrains power consumption, thereby limiting sensor designs, and sampling and communication duty cycles.

The Minimet drifter mechanical configuration is diagrammed in Fig. 2. Some of the Minimet drifter design and wind observing system heritage is already evident in the figure. Drifter structure, floatation, and drogue designs are direct descendants of the World Ocean Circulation Experiment–Tropical Oceans and Global Atmosphere (WOCE–TOGA) Lagrangian drifter systems described by Sybrandy and Niiler (1991). The acoustic hydrophone component is representative of the Wind Observation Through Ambient Noise (WOTAN) technology for wind speed observations in harsh conditions that had been demonstrated for moorings by Vagle et al. (1990), and in drifter systems for more benign environments by Nystuen and Selsor (1997). Previous observations of wind direction from drifting systems in rough seas have been made from large platforms that precluded simultaneous ocean current estimates. Such observations compare favorably with conventional moored buoys, and operational analysis from numerical weather prediction; $\pm 5°$ in the mean, $<15°$ standard deviations after discarding outliers (Large et al. 1995). As in the case of Minimet, these prior observations derive from vanes fixed to the floatation elements, and the use of histograms of wind direction to determine the most common direction. A primary Minimet innovation was to overcome the major technical difficulty of following the surface current while still remaining above the surface for time periods long enough to amply sense the surface wind (Niiler et al. 1987, 1995). The wind vane addition to the drifter spherical surface floatation and electronics housing is the external component of the new wind direction observing system developed for the Labrador Sea Minimet.

Sampling and communications configurations for Minimet drifters evolved from high-resolution, power consumptive systems used to calibrate engineering model Minimet drifters in the laboratory and in sea trials off California; to the hardened, low-power Minimet systems deployed in the Labrador Sea. The Labrador Sea systems transmit data in near–real time via System ARGOS satellite remote communications resources. Minimet observational records are refreshed every hour, and the most recent data record is transmitted nominally every 90 s. The System ARGOS coverage of the Labrador Sea region was such that, on average, hourly data were received about 14 times per day.

Wind direction observations derive from histograms of the wind vane orientation, in 5° bins, as sampled at 1 Hz for 160 s every hour. Details of the predeployment Minimet wind direction calibration are provided in the appendix. Under low- to medium-strength wind conditions, rms wind direction differences are between 6° and 8° for drifters within a few hundred meters of each other. Additional field calibrations for Minimet wind direction retrievals in the Labrador Sea deployment are described in section 3a below.

Minimet wind speed observations derive from acoustic pressure data collected by the WOTAN hydrophone and averaged in four batches of 5 min each, over a 20-min period, every hour. Within each batch, the acoustic pressure signal is sampled for 30 s each minute, and averaged. As detailed in the appendix, the Minimet wind speed calibration differs from the attempts by Vagle et al. (1990) for absolute wind speed calibration using WOTAN systems. Instead, a relative calibration with NSCAT is maintained over the field lifetime of each drifter in the Labrador Sea. Absolute calibration of WOTAN systems has not proven feasible when deployment locations differ (Vakkayil et al. 1996), or for multiple hydrophone systems in the same location (appendix).

While effective averaging times for Minimet wind speed (acoustic pressure amplitudes averaged over 20

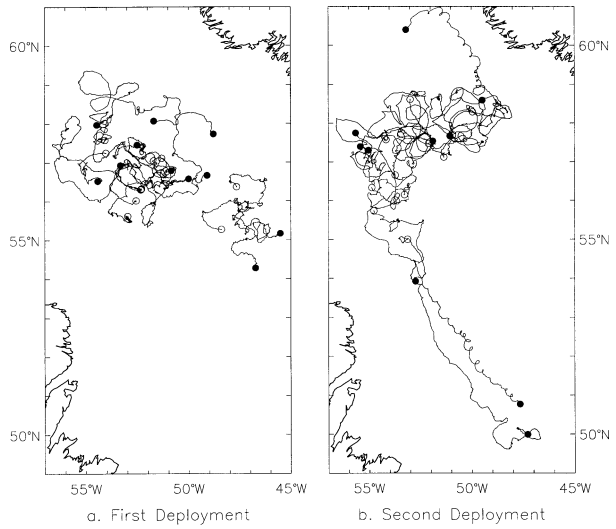

FIG. 3. Tracks of all Minimet drifters in (a) the first deployment (22 Oct 1996–3 Mar 1997), and (b) the second deployment (19 Feb 1997–28 May 1997). An ''x'' marks the deployment locations for each Minimet drifter, and circles mark Minimet drifter positions at the end of the observational record for each drifter.

min) and wind direction (160 s to collect each histogram) are different, they are both consistent with a low-pass filter to preserve mesoscale variability in the geophysical signals. The wind speed averaging timescale is at least a factor of 3 shorter than the mesoscale temporal signal of interest. Kaimal et al. (1972) demonstrate that microscale surface wind velocity components peak at frequencies up to two decades higher than the frequency corresponding to the averaging timescale for wind direction [appendix; see also Fig. 17 Kaimal et al. (1972)]. This means that the averaging times for wind direction and wind speed both fall in the spectral gap between microscale and mesoscale. So, for example, increasing to 20 min the interval over which the wind direction histogram is accumulated would increase power consumption and not change the results.

The Labrador Sea Deep Convection Experiment coincided with the calibration and validation period for NSCAT immediately following launch. Research vessels operating in this field program in the winter of 1996/97 provided transport and deployment opportunities for two separate arrays of Minimet drifters. Figure 3 depicts the drifter tracks for each deployment and Table 1 documents the data record lengths for each drifter. The first deployment roughly spans the period late October 1996 through February 1997, with substantial data records for wind direction from 11 Minimet drifters, and wind speed records for 8 drifters. Our primary focus will be on the wind direction data from this deployment, as it spans most of the winter season, and it is during this deployment that several drifters happened to be close enough to each other to measure wind variability over short distances. Table 1 summarizes separately the Minimet drifter wind direction and wind speed data coverage for the two Labrador Sea deployments. The average Minimet drifter wind direction data record spanned 89 days (with a range of 45–115 days). The wind speed observing systems failed on 4 of 21 Minimet drifters deployed in the Labrador Sea. Wind speed data records ended prematurely on six other drifters (Table 1).

The laboratory and field tests of engineering model Minimet drifters described in the appendix could not match the extremes in wind speed, wave state, and cold

TABLE 1. Minimet wind direction and speed data in first and second deployments. Listed are the dates of the entire wind direction data period, the number of days with direction data, the number of direction data, the number of days with speed data, and the number of speed data.

Drifter	Dates (mm/dd/yy)	Days_{dir}	N_{dir}	Days_{sp}	N_{sp}
16881	10/31/1996–01/24/1997	85.6	1189	—	—
16883	11/16/1996–01/01/1997	45.5	665	—	—
16886	10/24/1996–02/16/1997	114.5	1440	—	—
16887	10/25/1996–02/11/1997	109.1	1557	38.8	601
16890	10/26/1996–02/07/1197	104.6	1534	4.6	82
16891	10/22/1996–01/27/1997	97.0	1382	50.0	740
16892	10/30/1996–02/14/1997	106.9	1427	106.3	1421
16895	11/14/1996–03/02/1997	108.5	1651	97.7	1502
16896	10/25/1996–01/31/1997	98.1	1368	98.1	1399
16899	10/24/1996–02/03/1997	101.3	1302	101.3	1302
16905	10/25/1996–01/26/1997	93.7	1346	44.8	653
16898	03/02/1997–05/28/1997	87.2	1280	85.5	1261
16901	03/15/1997–05/22/1997	68.3	874	66.5	850
16902	03/12/1997–06/07/1997	87.6	1102	87.6	1130
16906	02/27/1997–05/11/1997	73.3	957	11.6	154
16907	02/19/1997–05/18/1997	88.5	1259	88.5	1268
16908	03/01/1997–05/14/1997	74.3	1069	73.3	1055
16909	02/26/1997–05/29/1997	91.9	1249	91.9	1249
16910	02/14/1997–05/23/1997	98.4	1332	98.4	1364
16911	02/25/1997–04/11/1997	45.1	631	—	—
24065	02/26/1997–05/18/1997	81.0	1193	14.6	212

temperatures that the Minimet drifters experienced in the Labrador Sea. In addition to these calibrations, we describe in the next sections how collocated NSCAT observations in the Labrador Sea were used to remove distortions in Minimet wind direction observations and to standardize Minimet wind speed observations derived from multiple WOTAN instruments. The collocation dataset includes all Minimet drifter and NSCAT wind observation pairs that occurred within 50 km and 60 min of each other. On average, there was one NSCAT collocation per day for each Minimet drifter. The Labrador Sea experimental plan included the deployment of a moored meteorological instrument array that could also have been used to calibrate the Minimet drifters with in situ data. Unfortunately, the moored system failed soon after deployment.

a. Minimet wind direction calibration with NSCAT

As described in the appendix, the prototype Minimet design included features that later proved to be incompatible in the creation of and sensitivity to local magnetic fields. The flux gate compass component of the wind direction observation system was sensitive to magnetic field effects from internal batteries and other magnetized components within the drifter housing. Also, the compass precalibrations to ameliorate the effects of internal magnetic fields appear to have been distorted by an external magnet applied to each Minimet drifter upon deployment to initiate the observation duty cycles.

Laboratory tests of fully assembled Minimet drifters demonstrated that the magnetic distortion was characterized by the superposition of a constant direction offset and distortion sidelobe effects. We describe here a procedure used to remove these distortions by fitting a calibration curve to the distribution of the NSCAT minus Minimet wind direction difference versus the raw Minimet wind direction. In order to apply the wind direction correction algorithm for the Minimet systems, a subset (N_{fit}) of the highest quality and most closely collocated data was defined to conservatively exclude conditions when either the Minimet drifter or NSCAT might have been reporting erroneous, or low accuracy, measurements. As an example, we review the refinement of the collocation dataset and calibration curve fit for Minimet drifter 16895 as depicted in Fig. 4. Similar refinements and wind direction calibrations were performed for each Minimet drifter and a summary is provided in Table 2.

First, the collocation subset was limited to data that were within 20 km, so that the Minimet observation originated from a location within an NSCAT WVC. For drifter 16895, Fig. 4 indicates that most of the collocated data are within this range. There are 21 data pairs with distances greater than 20 km (the squares in Fig. 4). A scatterplot of wind direction differences as a function of time differences (not shown) indicates that the wind direction difference does not increase with time difference for the range of spatial and temporal differences

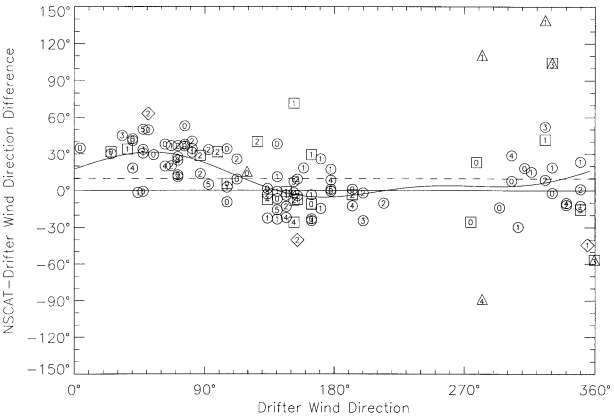

FIG. 4. Sample wind direction calibration diagram for Minimet drifter 16895. Wind direction difference (NSCAT − Minimet drifter) vs Minimet drifter wind direction is plotted for all collocations within 60 min and 50 km. Collocation symbols correspond to refinements in the collocation dataset used for Minimet calibration with NSCAT as described in the text. A priori refinements are depicted according to separation distance (squares), wind speed regime (triangles), and possible upwind/downwind ambiguity removal errors (diamonds). Numerals inside each symbol represent temporal separations in the NSCAT and Minimet collocations (multiply numerals by 10 min). The dashed line represents a uniform offset and the curve is the result of a fit of sine and cosine terms derived independently for each drifter (and reported in Table 2).

considered here. This is also apparent in Fig. 4, where the time differences for each collocation symbol are indicated by numerals to be multiplied by 10 min within each symbol. All collocations within 60 min of each other were included in N_{fit}. The calibrations were not found to be significantly changed if the collocations were restricted to time differences $\leq$ 30 min.

Second, N_{fit} was refined according to reliable wind speed ranges. On a global basis, the NSCAT wind retrievals are deemed most accurate for wind speeds of 3–30 m s^{-1} (NASA Scatterometer Project 1998). Wind direction observations are always problematic approaching the limit of zero wind speed where direction is undefined. Predeployment tests of engineering model Minimet drifters reported in the appendix (see Fig. 11) found that wind direction estimates were in better agreement with each other for wind speeds in the range 6–7 m s^{-1}, than for speeds of 2–3 m s^{-1}. At lower wind speeds, the wind direction observation by Minimet was more sensitive to contamination by swell effects. The scatterplot of all Minimet versus NSCAT wind direction differences as a function of wind speed (not shown here) demonstrates a few anomalously high differences between Minimet and NSCAT data at small wind speeds, but no other dependence on speed. So a minimum speed of 5 m s^{-1} is used to further limit the N_{fit} collocations. For drifter 16895 this resulted in six data being excluded from N_{fit}, as indicated by the triangles in Fig. 4.

Third, when the wind direction difference between drifter and NSCAT exceeded 90°, data were not used. The few large direction differences were assumed to be

TABLE 2. Minimet calibration coefficients for wind direction and speed. Listed are the number of collocated drifter and NSCAT data for each drifter, the number of collocated data used to fit the calibration function, the mean distance and the mean time difference of collocated data, and the resulting calibration coefficients. The wind speed calibration coefficients are based on the 1–2-kHz band.

		Wind direction								Wind speed		
Drifter	N_{co-loc}	N_{fit}	$\overline{\Delta X}$ (km)	$\overline{\Delta T}$ (min)	C_0	C_1	C_2	C_3	C_4	N_{fit}	S	I
16881	73	60	10	25	24.2	6.2	5.6	−8.4	−4.2	—	—	—
16883	43	25	11	20	−0.3	−28.5	6.1	4.2	−13.0	—	—	—
16886	96	68	10	22	−2.2	0.7	1.8	18.0	0.1	—	—	—
16887	105	70	10	23	14.7	2.5	10.3	−23.5	−6.9	39	0.062	2.069
16890	105	76	10	23	−4.8	12.4	−8.6	4.7	−13.8	6	0.067	1.592
16891	83	57	11	22	−3.0	−1.6	−3.6	4.5	−6.0	38	0.063	2.223
16892	91	64	11	23	12.2	9.2	−3.1	1.2	−1.7	88	0.072	2.743
16895	112	84	10	20	9.7	9.4	6.5	11.4	−3.5	97	0.066	2.364
16896	85	61	10	21	0.8	−0.6	3.0	−8.8	−6.2	83	0.064	1.881
16899	84	62	11	27	9.4	24.5	−0.4	−4.9	−10.1	81	0.061	2.411
16905	82	62	11	21	−0.9	−14.5	−25.1	28.8	−11.1	38	0.060	2.356
16898	87	52	10	24	−33.8	−28.2	−14.7	5.5	−3.9	81	0.074	1.531
16901	53	36	11	23	40.2	−6.6	−1.2	−13.1	−7.7	50	0.053	2.867
16902	61	39	10	22	−0.1	13.8	4.4	2.1	−4.1	61	0.063	2.615
16906	69	45	10	21	−10.7	6.5	−0.9	8.8	−3.6	13	0.049	4.563
16907	89	55	10	24	6.6	10.8	8.0	6.7	−11.4	85	0.065	2.696
16908	75	46	9	22	55.5	5.3	12.7	4.0	15.8	71	0.063	2.458
16909	80	56	10	22	−14.8	17.8	3.7	−12.6	−10.2	77	0.062	5.035
16910	89	67	11	28	9.7	10.1	−5.3	10.9	−8.3	90	0.063	2.346
16911	36	30	10	25	−45.0	10.8	2.7	−21.2	−22.7	—	—	—
24065	79	53	11	22	−4.4	−2.3	−15.9	24.3	−18.5	13	0.068	2.026
Avg	80	56	10	23						59		

due to erroneous NSCAT data suffering from an incorrect upwind/downwind ambiguity removal (e.g., see Gonzalez and Long 1999).

After these three a priori refinements on N_{fit}, the average direction difference and the standard deviation of the differences were computed. In a final refinement of N_{fit} before curve fitting, all collocated pairs for which the direction differences exceeded 2 standard deviations were eliminated. The remaining N_{fit} collocations (circles in Fig. 4) are used to determine five calibration coefficients in the function:

$$\begin{aligned}\mathrm{dir}_{\mathrm{NSCAT}} - \mathrm{dir}_{\mathrm{Minimet}} &= C_0 + C_1 \sin(\mathrm{dir}_{\mathrm{Minimet}}) + C_2 \sin(2 \times \mathrm{dir}_{\mathrm{Minimet}}) \\ &\quad + C_3 \cos(\mathrm{dir}_{\mathrm{Minimet}}) + C_4 \cos(2 \times \mathrm{dir}_{\mathrm{Minimet}}).\end{aligned}$$

This procedure was repeated for each drifter independently. The N_{fit} and coefficients C_n, where $n = 0, 1, 2, 3, 4$, are listed for the entire Minimet dataset in Table 2.

For drifter 16895, we began with 112 collocated data pairs, and used 84 pairs for calibration. For this subset, the average distance between drifter and NSCAT data was 10 km, and the average time difference between observations was 20 min. The resulting calibration function for drifter 16895 is shown in Fig. 4.

Over all Minimet drifters, the offset coefficients C_0, ranged between −45.0° and +55.5°. There is no consistent pattern in the variations for any of the C_n when compared drifter to drifter. Subsequently, we have learned that small changes in the internal placement relative to the compass of the potentially magnetized components, especially the battery pack, make a big difference in the relative magnetization of the fully assembled float. The magnetic activation switch was replaced by a mechanical switch in later Minimet designs.

b. Minimet wind speed calibration with NSCAT

The WOTAN technology of inferring near-surface wind speed from underwater acoustic noise is thoroughly discussed in Vagle et al. (1990). The relationships are empirical and have typically been either logarithmic or linear, where the noise is a broadband rms pressure. Here we use a different broadband measure, P_{Minimet}, that is the accumulations of from 50 to 100 narrowband measurements of rms acoutic pressure. This procedure is detailed in the appendix.

NSCAT wind speed is linearly regressed against P_{Minimet} (see appendix), in each of the eight broad frequency bands to determine the slope (S) and intercept (I) of the calibration (Table 2):

$$\mathrm{speed}_{\mathrm{NSCAT}} = SP_{\mathrm{Minimet}} + I.$$

Points that were more than 2 standard deviations off this initial fit were discarded and the linear fit was performed again. Those individual fits vary from drifter to drifter by 20% in slope, which may be indicative of the different hydrophone sensitivities and power amplification. Positive intercepts were attributed by Vagle et al. (1990) to a wind threshold required to drive the

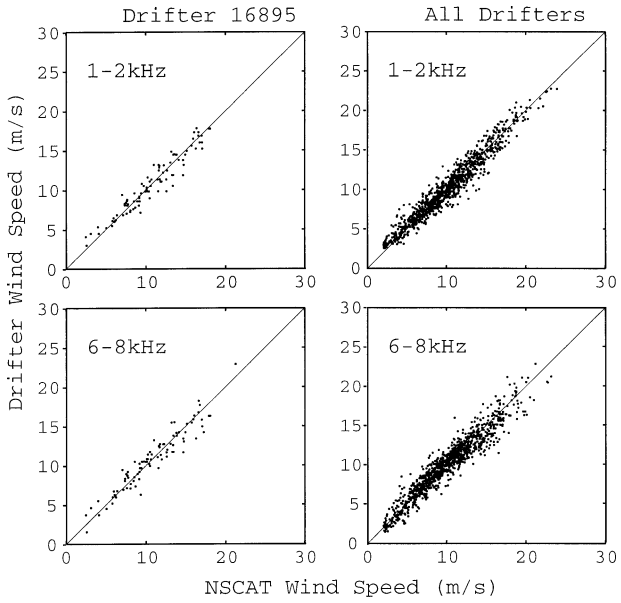

FIG. 5. Minimet wind speed calibration scatterplot comparisons with NSCAT wind speeds derived from the NSCAT–Ku2000 GMF. (left) Comparisons for Minimet drifter 16895 in the sound frequency bands (top) 1–2 kHz and (bottom) 6–8 kHz. (right) The combined scatterplots for all Minimet drifters in the Labrador Sea deployments.

physical mechanisms of noise generation (e.g., wave breaking). The more than 20% variation in the intercept may be related to the number and range of the wind speed data.

Figure 5 (left panels) depicts the linear fit for Minimet drifter 16895 versus collocated NSCAT for two frequency ranges: 1–2 kHz (top) and 6–8 kHz (bottom). For this drifter, it appears as if either band could be used for wind speed estimates, but there are few points above about 18 m s^{-1}. This situation improves when all drifters are considered (Fig. 5, right panels) and it appears as if linear Minimet calibrations hold to at least 20 m s^{-1} for frequencies less than 8 kHz, provided the NSCAT winds are valid up to this speed. Precipitation greatly increases acoustic noise at about 12 kHz, and there is sometimes a noticable increase at 8 kHz (Vagle et al. 1990). We adopted the common practice of avoiding contamination from precipitation noise by using only the 1–2-kHz band to retrieve wind speed.

The fidelity of the WOTAN response in the 6–8-kHz band to wind speeds as high as 20 m s^{-1} is somewhat unexpected. Farmer and Lemon (1984) attribute an observed high-frequency falloff in acoustic signal at high wind speeds to greater attenuation of the higher frequencies from bubbles produced near the ocean surface by breaking waves. The empirical rule from noise measurements at 150-m depth is that noise at 8 kHz is affected at speeds above about 15 m s^{-1} (Vagle et al. 1990). It appears as if this rule may not hold for the Labrador Sea WOTAN deployments, possibly because at depths less than about 20 m, selective trapping of the sound in the bubble layer is expected, even at frequencies as low as 1 kHz (Farmer and Vagle 1989). Further evidence for valid response at high wind speeds in the Labrador Sea WOTAN deployments can be taken from the ratio of the calibration for the 1–2-kHz band to that of the 6–8-kHz band. Averaged over all the Minimets of Table 2, this ratio is 2.0, which is consistent with the frequency dependency of acoustic power falling off as f^{-q}; for frequency f and exponent $q = 1.8$ here. This value is within, but on the low side, of the range of reported values of q: 1.7 (Lemon et al. 1984) and 2.2 (Bourassa 1984). Bubble attenuation would lead to a steeper falloff, or larger absolute value of q.

c. *Sample Minimet surface wind data for the Labrador Sea*

For the entire calibrated collocated dataset, now including the outliers not used in the individual calibrations, the scatterplot (not shown here) of all Minimet drifter wind speeds versus NSCAT indicates a residual bias of 0.1 m s^{-1}, with an rms of 2.0 m s^{-1}. Similarly for wind direction, the remaining bias is 1.4°, with an rms of 33.4°. Analysis of the wind direction rms is taken up in the sections to follow. For the remainder of this section we present sample results from the Labrador Sea Minimet drifter deployments.

Figure 6 depicts superpositions of Minimet drifter surface wind retrievals and NSCAT surface wind retrievals on two successive descending orbits (revs 1548 and 1549) at 1422 UTC (Fig. 6a) and 1h, 41 min later at 1603 UTC (Fig. 6b) on 3 December 1996. All 11 drifters in the first deployment are represented in the figure, and the Minimet retrievals all occur within about 30 min of the overpasses (before or after). Observations from the same drifter are either separated by 1 h (for seven drifters) or 2 h (four drifters). Thick, filled vectors represent Minimet drifter wind retrievals when both wind direction and speed were measured by the drifter. Thick, unfilled vectors use Minimet wind direction observations and nearest-neighbor NSCAT wind speed information. Overall, Minimet drifter wind directions exhibit more variability, both over the short time interval captured in Fig. 6 and over the spatial mesoscale. Several of the Minimet retrievals in Fig. 6 change much more in orientation than nearby NSCAT vectors over the time period between the two overflights. Moreover, for each overpass the NSCAT fields are much smoother than the Minimet vectors. The latter appears to be signal rather than noise, because in several instances wind vectors from nearby drifters differ in the same sense with respect to the NSCAT vector wind field.

Figure 7 depicts time series, over 110 days, of surface pressure (Fig. 7a), wind speed (Fig. 7b), and wind direction (Fig. 7c) from the observational record for Minimet drifter 16895. Similar figures (not shown here) were made for all the drifters listed in Table 1. Figure 7 has been chosen to be representative of the entire

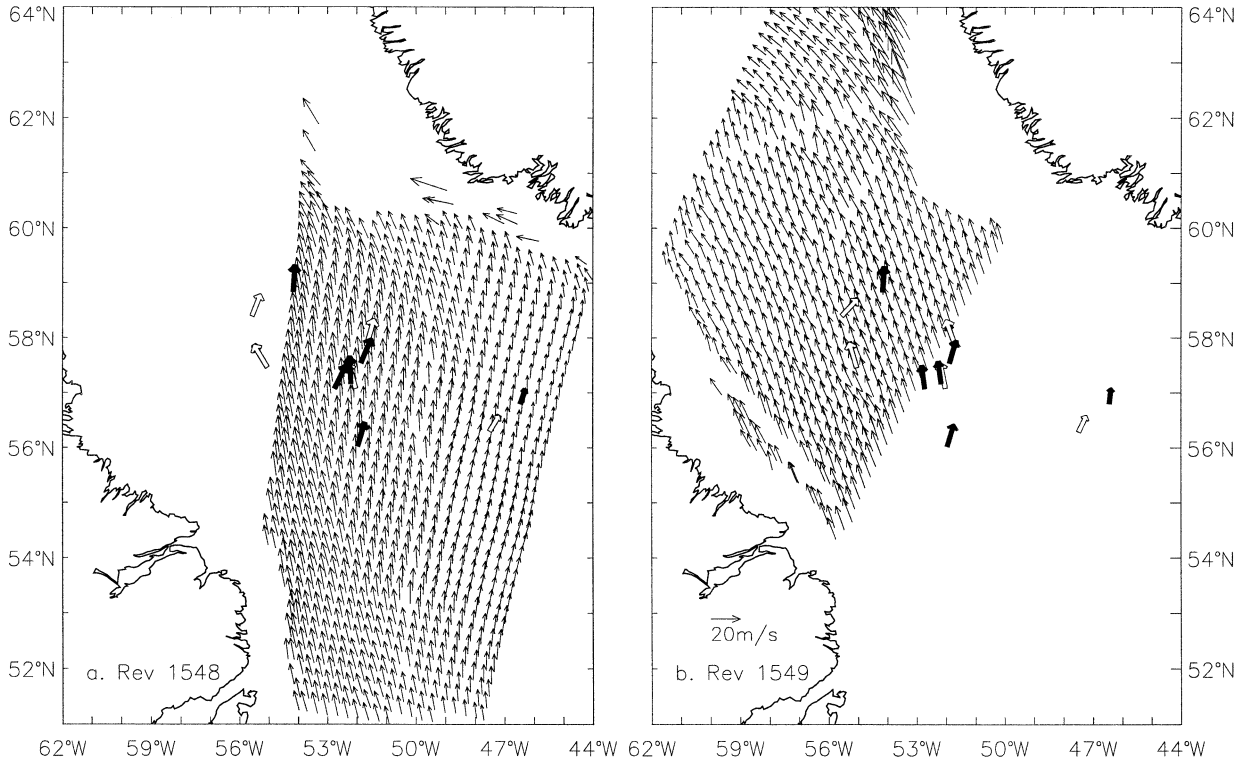

FIG. 6. Surface vector wind retrievals from consecutive NSCAT descending orbits and coincident Minimet drifters in the Labrador Sea on 3 Dec 1996 (a) at 1422 UTC for rev 1548, and (b) at 1603 UTC for rev 1549. In both panels the satellite moves from north to south. During rev 1548 the 600-km-wide right side of the swath (24 across-track WVC) covers most of the Labrador Sea. In the next revolution the left half of the swath overlaps with the previous swath. All 11 Minimets of the first Labrador Sea deployment are depicted in each panel. The Minimet observations all occurred within 37 min (before or after) of the first overpass, and again within 32 min of the second overpass. Filled vectors are data with drifter observed wind direction and speed, and unfilled vectors are observed drifter direction but nearest-neighbor NSCAT speed.

dataset. Open circles in the middle and bottom panels are the superposition of collocated NSCAT wind speed and wind direction retrievals, respectively.

Large-amplitude wind speed events in Fig. 7 often coincide with local surface pressure minima and abrupt changes in wind direction. These coincident changes are consistent with the development and propagation of synoptic-scale systems such as shown in Fig. 1. In fact, wind speed and direction observations for drifter 16895 account for the northernmost Minimet drifter vector in Fig. 1. The pressure and wind direction changes that correspond to the local wind speed maximum for the synoptic setting in Fig. 1 are evident around day 397 in Figs. 7a and 7c.

Note, however, that for a few large wind speed events (e.g., around days 393 and 409) the NSCAT retrievals substantially exceed the Minimet maxima with speed estimates greater than 30 m s^{-1}. Similarly, a few large-amplitude wind speed events in the Minimet record (e.g., around days 346 and 367) are not sampled by NSCAT. The Minimet wind speed estimate on day 367 is as large as 30 m s^{-1}. For the entire dataset, there are not sufficient numbers of coincident Minimet and NSCAT observations for wind speeds in excess of 25 m s^{-1} to either validate NSCAT retrievals with Minimet, or conversely, to conclude that Minimet wind speed sensitivity is saturating, at very high wind speeds. There are instances of coincident observations for wind speeds in excess of 20 m s^{-1} in Fig. 7 (e.g., around days 345 and 385); and as previously noted, Fig. 5 indicates that other drifter records contain coincident observations in the 20–25 m s^{-1} range as well.

The wind direction time history (Fig. 7c) is of particular interest. The efficacy of the wind direction calibration with NSCAT is demonstrated by instances of $O(100°)$ direction changes tracked by both instrument systems over intervals as short as the time span of successive overflights (e.g., day 380). Superposed on the direction variability that occurs on the order of days that is well represented in both NSCAT and Minimet records, there exists a much shorter timescale variability apparent in only the Minimet record. The amplitude of this higher frequency variability is $O(40°)$ and it occurs throughout the record in Fig. 7c, and is typical of wind direction time histories for all the Minimet drifters in the Labrador Sea deployments. This variability is also consistent with the visual distinctions between NSCAT and Minimet in Fig. 6. It is much larger in amplitude

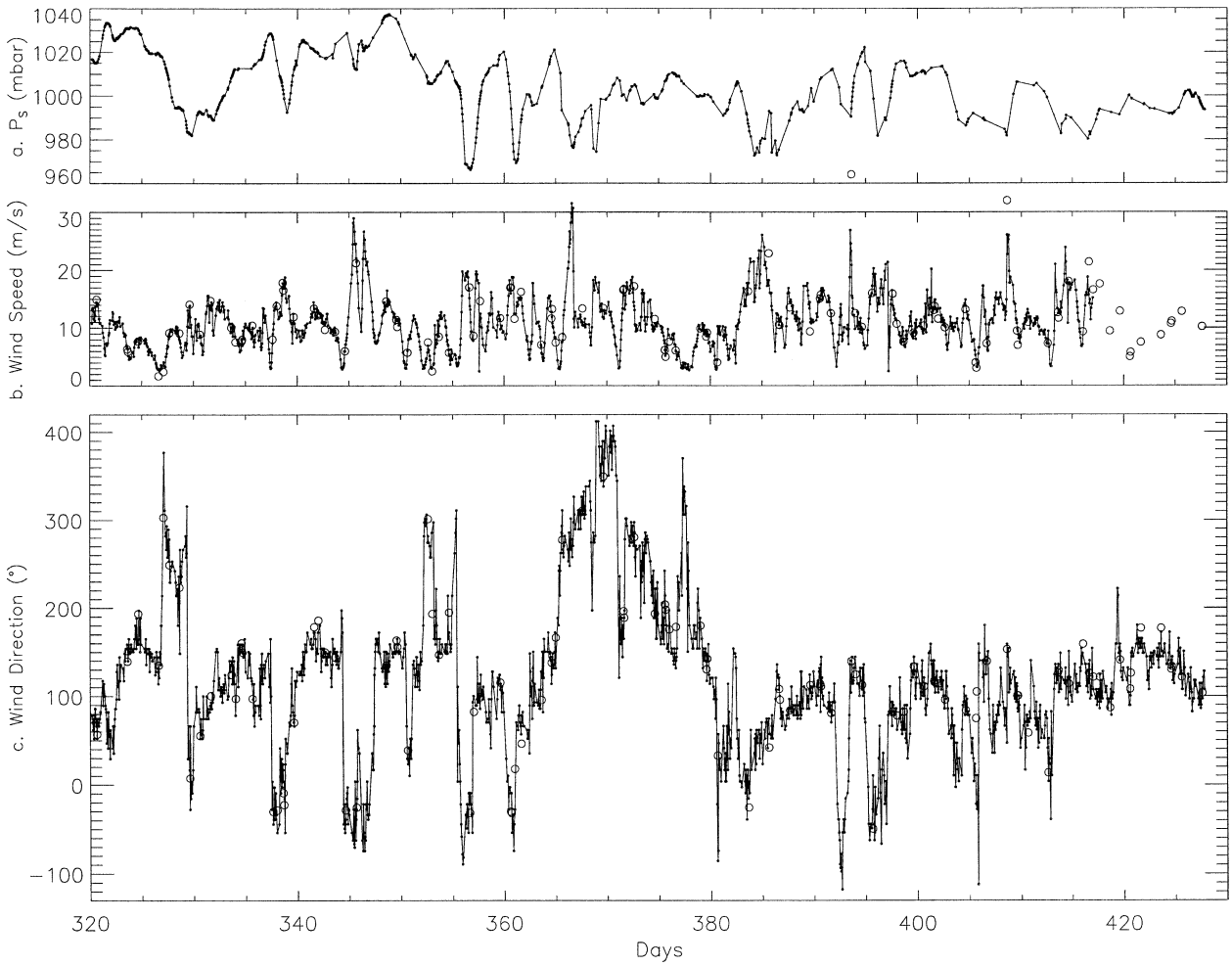

FIG. 7. Time series for drifter 16895 of (a) air pressure, (b) wind speed, and (c) wind direction for 110 days spanning much of the first Labrador Sea deployment. Open circles in wind speed and direction time series are for collocated NSCAT data as derived from the Ku2000 GMF.

than the uncertainty estimates (i.e., 6°–8°) for Minimet wind direction observations derived from the preliminary field calibrations described in the appendix.

4. Discussion

In this section, we take up the issues involved in comparing the Minimet and NSCAT datasets, which are not independent because of the Labrador Sea field calibrations for each Minimet drifter. It remains for us to quantify the visual inferences from Figs. 6 and 7 of shorter time- and space scale variability in the surface wind field that we associate with an energetic mesoscale. We argue this case in two ways. First, in differencing vector wind observations from Minimet drifters over a wide variety of synoptic conditions and spatial scales to reduce the amplitude of large-scale signals, and second by comparing records for Minimet drifter groups that were very near each other for periods of many days, under relatively constant large-scale wind conditions.

a. Rms differences versus spatial separation

Observations of the surface wind speed and direction variabilities as a function of spatial scale are represented as rms differences versus separation distance in Fig. 8. Each drifter record was compared against the records from all other drifters. Whenever observations from two different drifters occurred within 30 min of each other, the differences in wind speed and direction were assigned to the spatial separation bin corresponding to the separation distance at the time of the observations (bins discretized into 20-km intervals from 0 to 400 km). In order to concentrate on the winter season, the period of interest was restricted to November 1996 through March 1997.

The region of the Labrador Sea over which the speed and direction differences from NSCAT were accumulated was limited to match the subdomain occupied by the Minimet drifters (i.e., the central basin; see Fig. 3a). Even so, spatial coverage within the NSCAT swath is

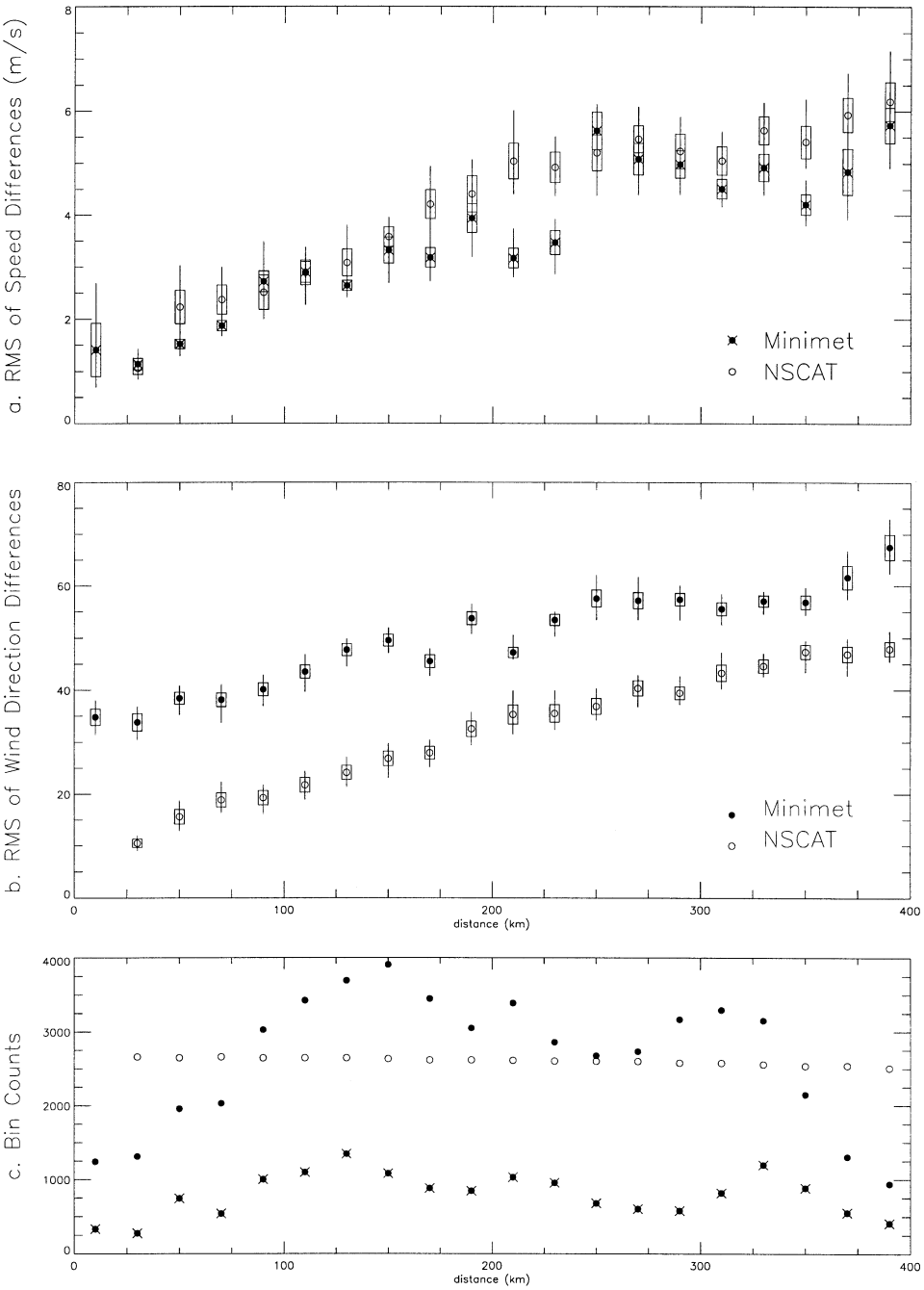

FIG. 8. Rms differences vs spatial separation for (a) wind speed and (b) wind direction from coincident fields of Minimet (filled circles) and NSCAT (open circles) observations. An estimate of the uncertainty (ranges indicated by vertical lines, and 1 std dev indicated by boxes) of the rms differences is provided as described in the text. (c) The number of differences (i.e., bin counts) for each spatial separation bin, for NSCAT (open circles, both speed and direction), Minimet wind directions (filled circles), and wind speeds (filled circles with x's).

dense and many more speed and direction differences are possible for spatial separations within the swath dimension. To balance the numbers of NSCAT and Minimet differences per spatial separation bin, NSCAT differences were randomly selected from the swath observations until the number of differences roughly matched the number of Minimet direction differences in each spatial separation bin (ca. 2600). The NSCAT rms values are found to be insensitive to increase of sample size by factors of 10 or even 100.

The Minimet and NSCAT bin counts used in Figs. 8a and 8b are shown in Fig. 8c. There are about 4 times as many Minimet wind direction difference pairs than there are Minimet wind speed difference pairs. For spatial separations between 0 and 20 km, only Minimet differences were possible, and there were 332 wind speed differences and 1242 wind direction differences for this bin. We selected more evenly distributed bin counts for the NSCAT differences in both speed and direction (Fig. 8c).

No account has been made of spatial and/or temporal dependence in the observations that comprise the differences from either observing system. This is not a crucial approximation in that while differences will not be independent for the same two drifters whose separation distances are within the same spatial separation bin over several hours, the bin counts attest to the fact that there are many such episodes for many different drifter pairs in the summaries presented in Fig. 8. Conversely, for the NSCAT differences, it is probable that differences over a wide range of spatial separation bins all taken from the same swath might not be independent (i.e., if the differences are reflective of the same synoptic-scale event). However, with $O(1000)$ differences in each bin, drawn uniformly from an observing period that spans more than 150 days and about 190 different satellite swaths, we are confident that no single synoptic event dominates the analysis. To be sure, we analyzed a subset of the drifter and NSCAT differences restricted to include only the difference pairs when both Minimet and nearby NSCAT wind estimates were available at the same times. While this limits the bin counts in many spatial separation bins to fewer than 100, the results to be described below are not significantly changed.

A bootstrap method for estimating the 1 standard deviation spread of the rms differences in speed and direction is depicted in Figs. 8a and 8b, respectively. To estimate the standard deviation in rms difference for each spatial separation bin the following procedure was implemented. The rms difference is recomputed 50 times from randomly drawn subsamples of the total populations of wind direction or wind speed differences in each bin. The subsample population sizes are set equal to one-half the respective bin counts. Boxes indicating 1 standard deviation in the rms difference are drawn for each circle (filled and open) in Figs. 8a and 8b. Vertical bars indicate the ranges of the rms difference estimates from the 50 subsamples in each bin. While the ranges vary somewhat depending upon the number of subsamples and/or the size of each subsample, the estimates for 1 standard deviation are more stable.

Figure 8a shows the rms difference for speed versus spatial separation; filled circles with ''x's'' represent the Minimet results for each spatial bin, and open circles represent NSCAT. Both datasets exhibit a linear increase in wind speed difference as a function of spatial separation out to at least 200-km separations (wind speed rms $\sim$ 4.5 m s^{-1}). The NSCAT differences continue in a linear trend of shallower slope to 400 km (NSCAT wind speed rms $\sim$ 6.0 m s^{-1}), while the Minimet drifter wind speed rms is widely scattered between 3 and 6 m s^{-1} for bins between 200 and 400 km. Both datasets are suggestive of an intercept of the y axis at about wind speed rms $\sim$ 1.0 m s^{-1}. These intercepts are within the global wind speed accuracy specifications for the NSCAT mission (NASA Scatterometer Project 1998).

We should also recognize that these rms intercepts are our best estimates of the combined instrument noise (different for each observing system) and natural variability of the surface wind speed in the Labrador Sea, in winter, at spatial scales too short to be well resolved by either observing system. This estimate of spatial-scale variability can be considered in light of short temporal-scale variability of the mesoscale surface wind field from Austin and Pierson (1999). In that study, the authors filtered time series of mesoscale observations from moored buoys in the North Atlantic and Gulf of Mexico, and compared the filtered and unfiltered data on scatterplots. Austin and Pierson (1999) found rms differences on the order of 1 m s^{-1} between the filtered and unfiltered datasets.

If we adopt for the case of mesoscale surface winds, a Taylor hypothesis as introduced for the microscale winds earlier, we can assume an equivalence between mesoscale temporal and mesoscale spatial fluctuations of the surface wind speed. In that case, the rms intercepts in Fig. 8a and the results of Austin and Pierson (1999) are roughly consistent. We note, however, assuming a Taylor hypothesis construct for the mesoscale surface wind field is very much an open question.

Figure 8a also demonstrates that the wind speed rms differences at short spatial separations are not useful to distinguish the sensitivities of Minimet or NSCAT systems to the mesoscale surface wind signal.

Figure 8b depicts the average rms differences in surface wind direction as a function of spatial separation distance; filled circles for the Minimet drifters, and open circles for randomly sampled NSCAT differences. The rms wind direction differences are significantly larger for Minimet comparisons than for NSCAT comparisons at all spatial separations. Moreover, the distinction in rms wind direction differences between the two observing systems is roughly constant at about 20° over a large range of spatial separations; for example, from 20 to almost 700 km (not shown). For the shortest spatial separations (20–40 km), the rms direction difference for NSCAT pairs is around 10°, while it is around 35° for Minimet comparisons. At 400 km, the average rms direction difference for NSCAT is about 45°, and for Minimet drifters, about 65°.

As in the case of the wind speed differences, in addition to the true mesoscale wind direction variability signal, these rms differences also contain a part due to noise in the observing systems. In the Minimet case, estimates of a noise term on the order of about 8° come from field tests off California with engineering model

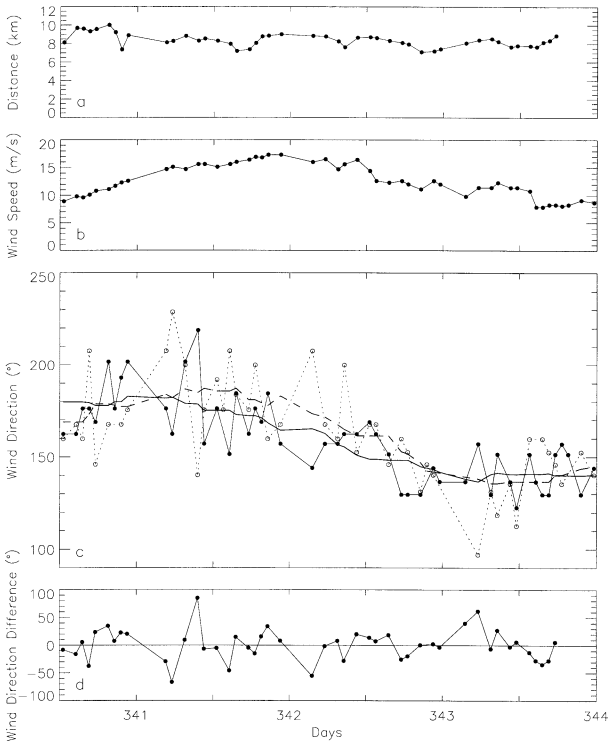

FIG. 9. Data record comparisons for nearby Minimet drifters 16896 and 16886. Panels depict time series for (a) separation distance, (b) wind speed from Minimet 16896 (no data from 16886), (c) wind direction (16896 filled circles, and 16886 open circles), and (d) wind direction difference over more than 4 days. (c) Smooth solid (for 16896) and dashed (for 16886) lines depict 12-h running mean wind direction time series. (d) The wind direction differences are computed after removing the respective 12-h running means.

Minimet drifters (appendix). To be careful, we let the Minimet wind direction observing system noise estimate in the Labrador Sea case be $O(10°)$ to account for any residual errors after the calibration with NSCAT directions.

b. Minimet records for drifters in close proximity

To further explore the signal-to-noise budget for the Labrador Sea Minimet wind direction observations, we compare records for Minimets that were very near each other in space (<12 km) and time (<30 min) during relatively constant wind events (speeds and directions) that occurred for longer than a day. A sample comparison of nearby Minimet drifter wind direction estimates is shown in Fig. 9. Minimet drifters 16886 and 16896 were within 10 km of each other for 3.5 days. The wind direction time series for each Minimet drifter are depicted in Fig. 9c. A half-day running mean direction trace is also shown for each drifter, and these demonstrate that the drifters are measuring the same synoptic-scale wind directions. In addition, there is a short time-scale variability in wind direction that differs between drifters even over this very short separation distance (average separation over the period is 8.4 km). The direction differences for the case shown in Fig. 9 are computed after removing the respective running mean directions. The time series of the differences is shown in Fig. 9d. The rms direction difference is 28.1° for this particular episode and drifter pair (see Table 3).

Five separate episodes, involving seven different drifters in 18 pairings, are summarized in Table 3. Also listed in the table are the rms differences in wind direction observations during these periods. The average

TABLE 3. Rms wind direction differences of nearby drifters during steady wind conditions. For each drifter pair the average distance, the average time difference, the average speed, the number of data, and the rms wind direction are listed. There are five separate events. The direction differences are based on drifter directions that are adjusted by the half-day running mean of each drifter (see Fig. 9d).

Drifter, pair	Days	Period (days)	$\overline{\Delta X}$ (km)	$\overline{\Delta T}$ (min)	$\overline{\text{Speed}}$ (m s^{-1})	N_{rms}	Dir_{rms}
16905, 16899	302.7–304.5	1.8	2.4	25	7.6	23	31.3
16905, 16887	302.7–304.5	1.8	9.4	29	7.6	26	37.4
16905, 16886	302.7–304.5	1.8	2.8	20	7.5	24	29.9
16899, 16887	302.7–304.5	1.8	10.1	10	7.7	22	36.1
16899, 16886	302.7–304.5	1.8	1.0	29	7.8	23	29.9
16887, 16886	302.7–304.5	1.8	9.7	24	7.7	24	19.2
16905, 16899	310.5–312.0	1.5	9.5	25	10.2	23	16.3
16905, 16887	310.5–312.0	1.5	10.1	29	10.4	24	19.6
16886, 16896	340.5–344.0	3.5	8.4	8	12.6	46	28.1
16891, 16896	342.8–344.1	1.3	9.3	33	10.0	13	12.1
16905, 16890	347.8–350.4	2.6	5.0	29	—	33	12.1
16891, 16886	348.3–350.6	2.3	9.3	16	—	32	18.3
16891, 16886	351.5–352.4	0.9	7.9	13	—	13	29.3
16891, 16886	353.2–354.6	1.4	9.2	15	—	24	22.1
16891, 16899	371.6–376.0	4.4	2.4	20	16.8	60	16.5
16891, 16899	376.4–380.0	3.6	3.0	20	7.7	47	28.5
16891, 16899	382.7–385.4	2.7	5.0	23	19.9	24	15.9
Total/avg		36.5/2.1	7.0	22	11.6	481/28	24.6

rms wind direction difference over 481 Minimet drifter pairs is 25°. Again, we have not accounted for temporal and spatial dependence in the sequences of paired observations used in this calculation, but rely instead upon the abundance of observations and the diversity of events to average the effects of these dependencies. In each of the cases examined, the 0.5-day running mean directions are very similar for the drifter pairs.

The proximity of the Minimet drifter pairs examined in Table 3 limits the feasible spatial scales for variability in the surface wind field. As such, the rms direction differences probably provide a lower bound on the part of the rms direction difference due to true mesoscale fluctuations in the surface wind field. Given our estimate of Minimet wind direction observing system instrument noise (10°), and the signal-plus-noise estimate from Table 3 (25°), an estimate of the mesoscale direction variability signal detected by the Minimet drifters in the Labrador Sea is about 23° (i.e., $23^2 \approx 25^2 - 10^2$). Again, given a Taylor hypothesis for mesoscale wind fluctuations on these scales, this estimate compares well with independent estimates of the mesoscale surface wind variability in the North Atlantic and Gulf of Mexico due to Austin and Pierson (1999). Their estimates for the standard deviation of wind direction based on temporal variability in moored buoy observations at 10-m height is 19.7°.

Figure 8b shows that the wind direction differences detected by NSCAT are much lower than Minimet estimates over all spatial separations. We relate this to the combined effects of compositing radar backscatter signals within each WVC, and the median filter method used to select among wind direction ambiguities that arise from the NSCAT–Ku2000 model function inversion. While the details of the median filter are beyond the scope of this paper, comparisons with coarse-resolution weather center analyses at the initial iteration, and comparisons with neighboring WVC directions in subsequent iterations of the median filter, are operations that smooth out spatial variability within the NSCAT swath. This removes a mesoscale signal in wind direction that is detectable in the Minimet observations [O(23°) rms].

The median filter and/or GMF inversions do not appear to affect in a similar way the NSCAT wind speed differences for short spatial separations. However, as we have noted, the rms of wind speed differences over short spatial separations is affected by the expected wind speed accuracy limits for NSCAT. As we have also noted, the ambiguous vectors that emerge from the GMF inversions typically do not vary in wind speed as much as wind direction. The median filter operation then serves to distinguish wind directions but not wind speeds among the ambiguities. It is consistent with the rms differences in Figs. 8a and 8b to suspect that mesoscale spatial variability in NSCAT wind speeds is not filtered, but it is filtered in wind direction.

c. Spatial correlation model estimates

The Minimet detection of the mesoscale wind field in the Labrador Sea can be extended to obtain estimates of the characteristic length scales for surface wind mesoscale variability for the winter of 1996/97. As in the case for wind speed and direction in Fig. 8, we can compare the rms differences in eastward (u) and northward (v) velocity components as functions of spatial separation. Separate spatial correlation models can then be fit for u and v, and correlation length scales estimated based on those fits. We revert to estimates based on velocity components because, unlike wind direction, u and v are scalar fields where possible amplitude differences are unbounded. This is important in the correlation function derivation described below. Moreover, constructing velocity component estimates from Minimet observations is consistent given that mesoscale variability has been preserved in both wind speed and direction retrievals.

To remove the large-scale climatological differences in u and v, the NSCAT wind vectors were averaged into 1° lat × 1° lon bins for the winter dataset in the Labrador Sea. Using the Minimet position information, we have removed the appropriate 1° winter-average u and v components from the Minimet components before computing the rms differences versus spatial separation.

In the following, we demonstrate the derivation of a spatial correlation model for an arbitrary spatially dependent scalar function, $f(\Delta x)$, where $\Delta x = x_i - x_j$. The rms difference in pairs of observations of f is given by

$$f_{\text{rms}}(\Delta x) = \left\{ \frac{1}{N} \sum_{j=1}^{N-1} [f(x) - f(x + \Delta x)]^2 \right\}^{1/2}. \quad (1)$$

Using this, form a quantity f^* as

$$f^* = \frac{1}{2}[f_{\text{rms}}]^2. \quad (2)$$

Then the expected value of f^* is

$$\begin{aligned} E[f^*] &= \frac{1}{2}\{E[f(x_i)^2] - 2E[f(x_i)]E[f(x_j)] \\ &\quad + E[f(x_j)^2]\} \\ &= \sigma^2 - \text{cov}[f(x_i),\ f(x_j)] \\ &= \sigma^2\{1 - \text{corr}[f(x_i),\ f(x_j)]\}, \end{aligned} \quad (3)$$

where $E[\,\cdot\,]$ is the expectation operator, σ^2 is the field variance, cov$[f(x_i),\ f(x_j)]$ is the spatial covariance function, and corr$[f(x_i),\ f(x_j)]$ is the spatial correlation function for $f(x)$. Assuming the general class of exponential spatial covariance models, we have

$$E[f^*] = \alpha - \beta \exp\left[\frac{-\Delta x}{\theta}\right]. \quad (4)$$

In the spatial statistics literature (e.g., Isaaks and Srivastava 1989), α is called the sill that corresponds to

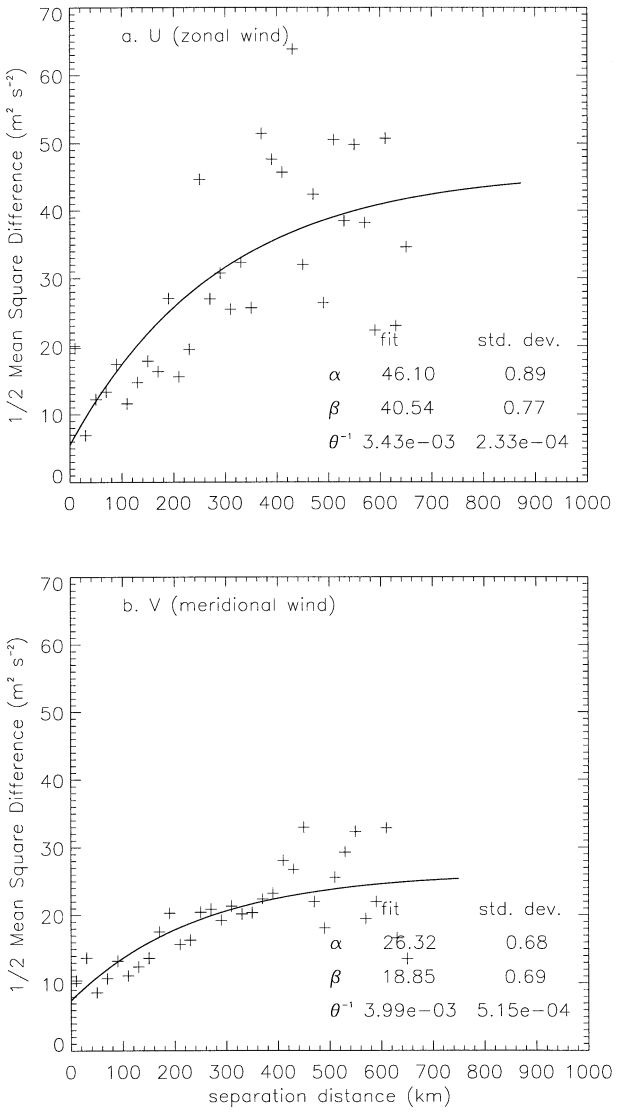

FIG. 10. Spatial correlation model fits for (a) zonal and (b) meridional wind component terms (e.g., u^* and v^* terms as described in the text). Plus signs indicate the scatter in each component as a function of spatial separation bin, and the curve is described by the spatial correlation model (4) in the text. Parameters and their std dev for the spatial correlation model are listed in each panel.

the field variance σ^2, and $\alpha - \beta$ is called the nugget, which is related to measurement uncertainty. The parameter θ is called the range and it is the e-folding scale for the exponential model for $E[f^*]$. The exponential model is fit such that at large $\Delta x > \theta$, $E[f^*]$ goes to the field variance; and at very small Δx, $E[f^*]$ goes to the nugget.

Figure 10 demonstrates the u^* (Fig. 10a) and v^* (Fig. 10b) versus spatial separation for the Minimet observations, and the corresponding exponential correlation model fits. Velocity component analyses require Minimet measurements of both wind speed and direction. This limits the bin counts for each spatial separation bin to the lower bin counts for wind speed described in Fig. 8c. However, the model fits are sensible and the model parameter estimates and uncertainties are listed in Fig. 10.

The correlation model fits are best for spatial separations from 0 to 400 km for both velocity components. Visual inspection of Fig. 10 indicates that the fit in v is better over that range than is the fit for u. Parameter uncertainties listed in Fig. 10 indicate that the fit in v is tighter over the entire range. The characteristic length scales (from estimates of θ) are about 290 km in the zonal direction and 250 km in the meridional direction. These scales are well within the range of the spatial scales over which rms differences were collected, and well spanned by the region of the Labrador Sea occupied by the drifters during the winter season.

The nugget values for u^* and v^* can be manipulated to compare with rms wind speed and wind direction differences at 0 separation in Figs. 8a and 8b. The nugget from the correlation model for u^* is about 5.5 m^2 s^{-2}, and the nugget for v^* is about 7.5 m^2 s^{-2}. If we double these and take square roots, we obtain units of rms, or 3.3 and 3.8 m s^{-1}, for u and v, respectively. These amplitudes are more than 3 times larger than the rms at 0 separation for wind speed differences in the Minimet drifter dataset. From what we have seen of the direction variability (e.g., Fig. 7), we can attribute most of the implied component amplitudes at 0 separation to the effects of wind direction variability.

The correlation model (4) is specific to spatial variability only. As such, the mesoscale surface wind length scale estimates do not account for temporal effects and the organization of coherent mesoscale structures in the wind field as described for Fig. 1. To account simultaneously for space–time variability is much more challenging, and even the combined Minimet and NSCAT datasets are not likely to be sufficient given standard methods. Common practice then resorts to methods of data assimilation wherein reinitializations and integrations of a numerical forecast model are required to constrain the field estimation problem. Alternatively, new approaches employing Bayesian hierarchical models are under development (Royle et al. 1999; Wikle et al. 1998; Wikle et al. 2001; Berliner et al. 2003).

5. Summary

Coincident estimates of the surface wind field in the Labrador Sea were retrieved from NSCAT observations and two deployments of Minimet drifters over the period October 1996–May 1997. The Minimet drifter represents a new technology for in situ observations of the surface wind field from ocean current following platforms in remote, and often harsh, environments. Minimet wind speeds are inferred from ambient acoustic noise (WOTAN), and a vane fixed to the surface float is used to infer wind direction.

Minimet drifter development and predeployment calibrations are reviewed in the appendix. The effective

temporal averaging of acoustic pressure signals, and the time interval over which a wind direction histogram is accumulated are shown to be consistent with low-pass filtering of microscale wind variabilities, and the preservation of the mesoscale.

Minimet drifters are designed to be inexpensive and power efficient so that many drifters can be deployed at a time to operate for a season or more. The Minimet drifter wind speed and direction observations have been calibrated with NSCAT. The relative calibration of drifting in situ systems with comparable observations from a spaceborne remote sensing system demonstrates a utility of the so-called modern ocean observing system (e.g., Smith and Koblinsky 2001). Such calibrations are carried out for the full field lifetime of the in situ systems, and therefore can involve many comparative measurements. Several deployments, in many different ocean basins, might one day be cross-calibrated in this way over the lifetime of the spaceborne observing system.

In the Labrador Sea case, a high-frequency O(hourly), large-amplitude $O(40°)$ variability in wind direction is evident in all Minimet time series after calibration with NSCAT (e.g., Fig. 7). An approximate signal-to-noise budget is possible given predeployment calibration data and multiple instances of multiday records from nearby drifter groupings in the Labrador Sea. Minimet wind direction instrument noise is probably less than 10°. Mesoscale surface wind direction temporal variability occurs on hourly timescales, and with typical amplitudes around 23°.

Variability of this kind is consistent with estimates for mesoscale wind variability from independent analyses based on single-point moorings in other ocean regions (Austin and Pierson 1999). This consistency depends upon a heretofore unsubstantiated assumption that mesoscale temporal and spatial variability are equivalent in the sense of a Taylor hypothesis. We note that several field campaigns, involving multiple Minimet deployments in a variety of surface wind regimes, could be used to test such an assumption for mesoscale surface wind variability.

A spatial correlation model fit to rms wind direction differences versus spatial separation yields estimates of the spatial scale of variability in the surface mesoscale wind for the Labrador Sea in winter. The estimated length scales are 290 km in the zonal direction and 250 km in the meridional direction. Estimates for the meridional length scale are less noisy than for the zonal scale. These estimates do not account for mesoscale temporal variabilities that are not well enough resolved in the combined Minimet and NSCAT datasets for use in conventional space–time models. Nonetheless, these length scales are consistent with the dimensions of coherent mesoscale regimes identified in different sectors of a polar low synoptic circulation system (Fig. 1).

To the extent that the Minimet wind speed observations have been standardized in the Labrador Sea deployments, there is validation information available with respect to NSCAT. The calibration of Minimet response in the 1–2 kHz band for wind speeds in the 20–25 m s^{-1} range of the Labrador Sea observations does not differ from calibrations for lower wind speed ranges (Figs. 5 and 7). This implies a consistency and validity in the NSCAT retrievals at these higher wind speeds where validation data are difficult to obtain. In terms of limitations of the NSCAT dataset, we have demonstrated that a mesoscale variability in surface wind direction is smoothed out of the NSCAT retrievals, possibly in the compositing of multiple backscatter returns over each WVC, and/or in the median filter step of the NSCAT processing used to resolve directional ambiguities. Finally, even in the case of the unprecedented abundance of surface wind field data for the Labrador Sea from NSCAT, the Minimet records demonstrate that several large-amplitude wind events are missed by the coverage capabilities of a single scatterometer platform.

Acknowledgments. The authors have all benefited, directly or indirectly, from the NASA Ocean Vector Winds program support and data. We thank Prof. M. H. Freilich and Drs. E. Lindstrom and W. T. Liu for NASA Science Working Team support through Oregon State University and the Jet Propulsion Laboratory. We thank Prof. W. Kendall Melville and Dr. Winfield Hill for advice regarding WOTAN observations and calibrations. We appreciate the efforts of the captain, crew, and scientific party of the *R/V Knorr* in deployments of the Minimet drifters in the Labrador Sea. Dr. Ian Renfrew is acknowledged for contributing AVHRR imagery in support of this work. Three anonymous reviews served to improve this paper.

APPENDIX

Minimet Drifter Design and Calibration

In order to characterize the spatial structure of strong mesoscale ocean winds as well as the ocean circulation they produce in the Labrador Sea, we set out to develop, build, calibrate, and deploy arrays of Lagrangian drifting buoys from which wind speed and direction would be returned in near–real time via the ARGOS system. Current following surface drifters cannot be overly exposed to the wind, and so have not previously been able to measure the surface wind. The WOTAN technology offered a potential technique for wind speed observations in severe conditions (Vagle et al. 1990). Using an upward-pointing, underwater hydrophone, the WOTAN system senses the ambient noise energy in the 1–22-kHz band that is known to be a function of the surface wind (Knudsen et al. 1948). A new wind vane and compass system has been developed to provide wind direction from Minimet drifters, without contamination of the drifter's current following capability. The Surface Velocity Programme Barometer (SVP-B) drifter (Sy-

brandy et al. 1995), which evolved from the WOCE–TOGA Lagrangian drifter (Sybrandy and Niiler 1991), offered a rugged, lightweight platform to which a WOTAN and wind vane could be attached, giving rise to the Minimet drifter design that was implemented for the Labrador Sea.

Prior to deployment in the Labrador Sea field experiment, laboratory, and field calibrations were needed to prove that accurate vector wind observations could be made, and to ensure that the data return was stable over a reasonable period of time. Field calibrations of Minimet engineering test models were conducted off California under a limited variety of surface wind conditions for which ship operations were feasible. An effort to calibrate the hydrophone response to acoustic noise across several instruments was not successful, as detailed in section 6c. This problem and the conclusion of Vakkayil et al. (1996) that known frequency-dependent correction factors are not adequate to account for site-to-site differences in the wind speed to noise relationship, means that in situ calibration (section 3b) is a necessity. There are several reasons why the Labrador Sea WOTAN ''site'' might be significantly different from others; two of which include the absence of low-frequency shipping noise and the shallow depth (10 m) of the hydrophone (Fig. 2). Ideally these issues will someday be resolved, so that absolute calibrations can de determined and independent WOTAN wind speeds can be returned directly from drifters and other platforms.

a. Mechanical configuration

Figure 2 depicts the Labrador Sea Minimet drifter configuration. Its design is based on the SVP-B drifter, to which are added wind speed and wind direction observing systems. The SVP-B drifter comprises a spherical surface float with a barometer port and a submergence switch on its top hemisphere, an SST sensor, and a magnetic startup switch on the lower hemisphere, and a urethane impregnated steel wire tether to a holey-sock drogue centered at 15-m depth. The startup switch is activated at the time of deployment with an external magnet to start the data measurement/recording cycle. The wind vane is attached both to the float and barometer port and almost never extends beyond 50 cm above the water surface.

The surface float houses the barometer sensor, digital controller, and ARGOS transmitter. The tether to the drogue is chained to a water-blocked and copper-screened cable with nine conductors and a 5/32-in. steel cable at its core. The conducting cable is terminated at a hydrophone cage to which is attached a drogue via a swivel. Without the swivel the wind vane was observed not to rotate into the wind direction. In addition to the electronic components of the SVP-B, the Minimet has a preamplifier in the hydrophone cage, as well as a signal conditioner (prewhitener), an FFT board, and a flux gate compass in the float.

b. Sampling and data processing

Data from the sensors are sampled on a repeated hourly cycle. The sampling begins 20 min before the hour, when the acoustic signal from the hydrophone is sampled over a 30-s period at 44.6 kHz. A portion of these digital data are divided into 100 subsegments of 2048 samples each. For each subsegment, the FFT board calculates the signal variance in 1024 frequency bands of width 0.022 kHz. At each frequency, this variance is directly related to the variance of the acoustic pressure fluctuations through the hydrophone sensitivity and electronics gain. The square root of the pressure variance gives the rms pressure, p_{rms}, over each frequency band. Vagle et al. (1990) established empirical relations that P_{rms}^2 falls as frequency to the power of -2, and varies linearly with wind stress magnitude. They further found that P_{rms} at a fixed frequency above about 1 kHz, varies linearly with wind speed.

In the Minimet system, the square root of the signal variance is summed over eight frequency bands: 1–2, 2–4, 4–6, 6–8, 8–12, 12–16, 16–20, and 20–22 kHz, then averaged over the 100 subsegments. This process is repeated every minute, and 5-min averages are formed. At the end of the 20-min sampling interval, four such 5-min averages of all eight frequency bands are transmitted to ARGOS satellites. Finally, processing of the data received by ARGOS combines all the 5-min averages that pass quality control into one average Minimet acoustic pressure, P_{Minimet}, which then can be converted to wind speed following the in situ calibration of section 3b. This broadband pressure is formed by accumulating P_{rms} then time averaging; whereas accumulating variance over a broadband, then time averaging the square root would give a pressure measure consistent with the P_0 of Vagle et al. (1990). During research vessel calibration studies (section 6c, below), raw acoustic data were recorded in the surface float of two engineering Minimet drifters. These data were processed with both the above-broadband accumulation methods, so that linear regressions against ship wind speeds could be developed for both. In effect, we were able to show that the variance of spectral estimates across 1–4-kHz bands increases with wind speed, such that both P_{Minimet} (Fig. 5) and P_0 (Vagle et al. 1990) vary linearly with wind speed. However, in developing universal algorithms to avoid in situ calibrations, variance accumulation over broadbands is preferable and will be incorporated in future Mimimet deployments.

The flux gate compass and the barometer sampling is done simultaneously, commencing 4 min before the hour, at 1 Hz for 160 s. The low duty cycle is necessary to conserve the limited power available. The 160 directions are placed into 5° bins, and the bin with the largest number of observations is recorded as the wind

direction. At a measurement height of 50 cm, and wind speed greater than 1 m s^{-1}, the peak in the microscale spectra of wind components (Kaimal et al. 1972) is found at periods shorter than 5 s. Therefore, the wind direction sampling window of 160 s is well within the spectral gap between the microscale and mesoscale, as is the 20-min wind speed averaging interval. Since the wind speed and wind direction both average over the microscale, their mesoscale variabilities are consistent and derived zonal and meridional wind components (u, v) are physically meaningful.

The four lowest pressures of the barometer samples are selected, and a median is constructed. If only one pressure falls below the median it is chosen as the air pressure reading, otherwise the two lowest values are averaged. This procedure minimizes contamination from erroneously high pressures due to submergence. Sea surface temperature is sampled every minute and 15 of these are averaged to update the SST file four times per hour.

The data for wind speed, wind direction, SST, and air pressure are updated every hour on a two-page format of the ARGOS data message. The two pages are broadcast alternatively every 85–90 s, depending on the cycle period assigned by Service ARGOS. Thus, these hourly data are transmitted every 170–180 s for 2 h. Transmission errors can be identified by the use of several checksums entered into each data page. During a nominal 15-min over-flight, Service ARGOS receives up to three different hourly updates and fixes several positions by Doppler ranging. A single location is determined with an uncertainty usually less than 350 m, but as large as 1 km, depending on the number of fixes that pass quality control set up by Service ARGOS.

c. Predeployment field tests

During calibration sea trials off San Diego, California, the research vessel was fitted with a mast on its bow. At a height of 10 m above the mean water line, two R. M. Young No. 05106 wind sensors were attached to cross members on the mast. Vector wind velocity from the R. M. Young sensors was sampled at 1 Hz and average values of both wind components were recorded every minute. Minimets were deployed within 100 m or less of each other, and the ship would stand within sight of these with the bow to the wind when observing wind direction. The drifters would still be within a few hundred meters of each other 2–4 h later. For wind speed comparisons, the ship would stand off at least 1 km so as not to interfere with the wind-produced acoustic noise. In these calibration studies, raw acoustic data was recorded at a 44.6-kHz sampling rate and the direction data was recorded at 5 Hz.

Visual observations of the Minimet floats from the ship revealed that the float would be pulled under water during passage of both swell and wind waves with no discernible periodic pattern. In the wave troughs the vane on the float would be oriented at random angles to the wind direction. Cresting the waves the vane would be aligned with the wind direction. During wind conditions of up to 11 m s^{-1}, when visual observations could be made, the wind vane would spend a noticeable time oriented in the wind direction. Several times floats were attached to the drogue with no swivels, and vanes on these floats would become oriented for long times at some random angle to the wind.

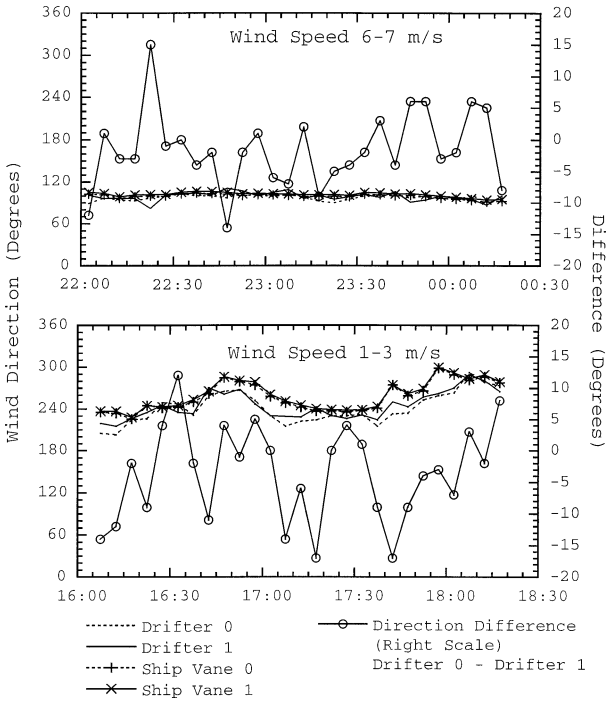

FIG. A1. Predeployment tests of two engineering Minimet drifters off California, when within 100–300 m of each other. Time series of wind direction when wind speeds ranged from (top) 6 to 7 m s^{-1} and (bottom) from 1 to 3 m s^{-1}. In each panel the drifter wind direction time series as well as time series from two ship anemometers are shown. The raw direction time series correspond to the vertical axes on the left-hand margins. In addition, the Minimet wind direction differences are plotted with respect to the right-hand axes. Rms of wind direction differences is (top) 6° and (bottom) 8°.

The ship calibrations were crucial in establishing that wind direction could be determined from drifter floats that submerged a significant fraction of the time and the magnitude of the instrumental and sampling noise level. Figure A1 displays the most likely directions over 160 s, sampled every 5 min, as computed from two separate deployments where two Minimets were in the water within a few hundred meters of each other. For comparison, the ship wind directions from an average of both R. M. Young sensors were computed for the identical 5-min period from the 1-min vector averaged observations. The rms direction differences between the two Minimets was 8° and 6° for wind speeds of 1–3 and 6–7 m s^{-1}. Therefore, we take 8° as a typical instrument noise, but this is likely an overestimate, because of the real turbulent microscale variability ex-

pected for 5-min samples, 100 m apart. For comparison, Large et al. (1995) report 17°–55° standard deviations between hour averages of drifter and moored direction measurements separated by as much as 100 km.

Absolute wind speed calibrations proved to be more problematic, both in the laboratory and in the field. First, it became evident that either the construction of the hydrophone housings or the hydrophones themselves were not identical as individual WOTAN instruments would show a significantly different response to the wind from an average of a group of WOTAN instruments. This occurred despite our efforts to select ''equivalent'' response hydrophones from the lot sent by the manufacturer by measuring their acoustic response functions in a controlled laboratory environment. Second, we found it not possible to recover drifters in wind speed conditions greater than 12 m s^{-1} and thus could not obtain data from a wide range of open ocean winds from our small research vessel. Third, the ship noise off San Diego severely hampered finding stable calibrations in the lower two frequency bands. These bands had historically been shown to be most effective in determining winds above 8 m s^{-1} and had been relatively insensitive to noise from precipitation.

REFERENCES

Atlas, R., S. C. Bloom, R. N. Hoffman, E. Brin, J. Ardizzone, J. Terry, D. Bungato, and J. C. Jusem, 1999: Geophysical validation of NSCAT winds using atmospheric data analyses. *J. Geophys. Res.,* **104,** 11 405–11 424.

Austin, S., and W. J. Pierson, 1999: Mesoscale and synoptic-scale effects on the validation of NSCAT winds by means of buoy reports. *J. Geophys. Res.,* **104** (C5), 11 437–11 447.

Berliner, L. M., R. F. Milliff, and C. K. Wikle, 2003: Bayesian hierarchical modelling of air–sea interaction. *J. Geophys. Res.,* **108,** doi:10.1029/2002JC001413.

Bourassa, S. L., 1984: Measurement of oceanic wind speed using acoustic ambient sea noise. Masters thesis, Graduate School of Oceanography, University of Rhode Island, 106 pp.

——, M. H. Freilich, D. M. Legler, W. T. Liu, and J. J. O'Brien, 1997: Wind observations from new satellite and research vessels agree. *EOS, Trans. Amer. Geophys. Union,* **78,** 597.

Brown, R. A., 2000: On satellite scatterometer model functions. *J. Geophys. Res.,* **105** (D23), 29 195–29 205.

Dickinson, S., K. A. Kelly, M. J. Caruso, and M. J. McPhaden, 2001: Comparisons between the TAO buoy and NASA scatterometer wind vectors. *J. Atmos. Oceanic Technol.,* **18,** 799–806.

Farmer, D. M., and D. D. Lemon, 1984: The influence of bubbles on ambient noise in the ocean and high wind speeds. *J. Phys. Oceanogr.,* **14,** 1761–1777.

——, and S. Vagle, 1989: Waveguide propagation of ambient sound in the ocean surface bubble layer. *J. Acoust. Soc. Amer.,* **86,** 1897–1908.

Freilich, M. H., and R. S. Dunbar, 1993a: Derivation of satellite wind model functions using operational surface wind analyses: An altimeter example. *J. Geophys. Res.,* **98,** 14 633–14 649.

——, and ——, 1993b: A preliminary C-band scatterometer model function for the *ERS-1* AMI instrument. *Proc. of the First ERS-1 Symposium,* European Space Agency, Special Publication ESA SP-359, 79–84.

——, and P. G. Challenor, 1994: A new approach for determining fully empirical altimeter wind speed model functions. *J. Geophys. Res.,* **99,** 25 051–25 062.

——, and R. S. Dunbar, 1999: The accuracy of the NSCAT 1 vector winds: Comparisons with National Data Buoy Center buoys. *J. Geophys. Res.,* **104,** 11 231–11 246.

Gonzales, A. E., and D. G. Long, 1999: An assessment of NSCAT ambiguity removal. *J. Geophys. Res.,* **104** (C5), 11 449–11 457.

Isaaks, E. H., and R. M. Srivastava, 1989: *An Introduction to Applied Geostatistics.* Oxford University Press, 561 pp.

Jones, W. L., L. C. Schroeder, D. H. Boggs, E. M. Bracalente, R. A. Brown, G. J. Dame, W. J. Pierson, and F. J. Wentz, 1982: The Seasat-A satellite scatterometer: The geophysical evaluation of remotely sensed wind vectors over the ocean. *J. Geophys. Res.,* **87** (C5), 3297–3317.

——, V. J. Cardone, W. J. Pierson, J. Zec, L. P. Rice, A. Cox, and W. B. Sylvester, 1999: NSCAT high-resolution surface wind measurements in Typhoon Violet. *J. Geophys. Res.,* **104** (C5), 11 247–11 259.

Kaimal, J. C., J. C. Wyngaard, Y. Izumi, and O. R. Cote, 1972: Spectral characteristics of surface-layer turbulence. *Quart. J. Roy. Meteor. Soc.,* **98,** 563–589.

Knudsen, V. O., R. S. Alford, and J. W. Emling, 1948: Underwater ambient noise. *J. Mar. Res.,* **22,** 410–429.

Lab Sea Group, 1998: The Labrador Sea deep convection experiment. *Bull. Amer. Meteor. Soc.,* **79,** 2033–2058.

Large, W. G., J. Morzel, and G. B. Crawford, 1995: Accounting for surface wave distortion of the marine wind profile in low-level Ocean Storms wind measurements. *J. Phys. Oceanogr.,* **25,** 2959–2971.

Lemon, D. D., D. M. Farmer, and D. R. Watts, 1984: Acoustic measurements of wind speed and precipitation over a continental shelf. *J. Geophys. Res.,* **89,** 3462–3472.

Liu, W. T., W. Tang, and P. S. Polito, 1998: NASA scatterometer provides global ocean surface wind fields with more structures than numerical weather prediction. *Geophys. Res. Lett.,* **25,** 761–764.

Lumley, J. I., and H. A. Panofsky, 1964: *The Structure of Atmospheric Turbulence.* John Wiley and Sons, 239 pp.

Mejia, C., F. Badran, A. Bentamy, M. Crepon, S. Thiria, and N. Tran, 1999: Determination of the geophysical model function of NSCAT and its corresponding variance by the use of neural networks. *J. Geophys. Res.,* **104,** 11 539–11 556.

Milliff, R. F., M. H. Freilich, W. T. Liu, R. Atlas, and W. G. Large, 2001: Global ocean surface vector wind observations from space. *Observing the Oceans in the 21st Century,* C. J. Koblinsky and N. R. Smith, Eds., GODAE Project Office and Bureau of Meteorology, 102–119.

Naderi, F. M., M. H. Freilich, and D. G. Long, 1991: Spaceborne measurement of wind velocity over the ocean: An overview of the NSCAT scatterometer system. *Proc. IEEE,* **79,** 850–866.

NASA Scatterometer Project, 1998: Science data product (NSCAT-2) user's manual: Overview and geophysical data products, Version 1.2. Jet Propulsion Laboratory, California Institute of Technology, D-12985, 78 pp.

Niiler, P. P., R. E. Davis, and H. J. White, 1987: Water-following characteristics of a mixed layer drifter. *Deep-Sea Res.,* **34,** 1867–1881.

——, A. L. Sybrandy, K. Bi, P. Poulain, and D. Bitterman, 1995: Measurements of the water-following capability of Holey-sock and TRISTAR drifters. *Deep-Sea Res.,* **42A,** 1951–1964.

Nystuen, J. A., and H. D. Selsor, 1997: Weather Classification using passive acoustic drifters. *J. Atmos. Oceanic Technol.,* **14,** 656–666.

O'Brien, J. J., 1999: Preface: Special section on NSCAT validation and science. *J. Geophys. Res.,* **104C,** 11 229.

Pagowski, M., and G. W. K. Moore, 2001: A numerical study of an extreme cold-air outbreak over the Labrador Sea: Sea, ice, air–sea interaction, and development of polar lows. *Mon. Wea. Rev.,* **129,** 47–72.

Pierson, W. J., 1983: The measurement of the synoptic scale wind over the ocean. *J. Geophys. Res.,* **88,** 1683–1708.

Renfrew, I. A., and G. W. K. Moore, 1999: An extreme cold air

outbreak over the Labrador Sea: Roll vortices and air–sea interaction. *Mon. Wea. Rev.*, **127,** 2379–2394.
——, G. W. K. Moore, T. R. Holt, S. W. Chang, and P. Guest, 1999: Mesoscale forecasting during a field program: Meteorological support of the Labrador Sea Deep Convection Experiment. *Bull. Amer. Meteor. Soc.*, **80,** 605–620.
Royle, J. A., L. M. Berliner, C. K. Wikle, and R. F. Milliff, 1999: A hierarchical spatial model for constructing wind fields from scatterometer data in the Labrador Sea. *Case Studies in Bayesian Statistics*, C. Gatsonis et al., Eds., Springer-Verlag, 367–382.
Schlax, M. G., D. B. Chelton, and M. H. Freilich, 2001: Sampling errors in wind fields constructed from single and tandem scatterometer datasets. *J. Atmos. Oceanic Technol.*, **18,** 1014–1036.
Shaffer, S. J., R. S. Dunbar, S. V. Hsiao, and D. G. Long, 1991: A median-filter-based ambiguity removal algorithm for NSCAT. *IEEE Trans. Geosci. Remote Sens.*, **29,** 167–174.
Shultz, H., 1990: A circular median filter for resolving directional ambiguities retrieved from spaceborne scatterometer data. *J. Geophys. Res.*, **95,** 5291–5303.
Smith, N. R., and C. J. Koblinsky, 2001: The ocean observing system for the 21st century: A consensus statement. *Observing the Oceans in the 21st Century*, C. J. Koblinsky and N. R. Smith, Eds., GODAE Project Office and Bureau of Meteorology, 1–25.
Stoffelen, A., and D. Anderson, 1997: Scatterometer data interpretation: Measurement space and inversion. *J. Atmos. Oceanic Technol.*, **14,** 1298–1313.
Sybrandy, A. L., and P. P. Niiler, 1991: The WOCE/TOGA Lagrangian drifter construction manual. University of California, San Diego, SIO 91-6, WOCE Rep. 63, 58 pp.
——, C. Martin, P. P. Niiler, E. Charpentier, and D. T. Meldrum, 1995: WOCE surface velocity programme barometer drifter construction manual, Version 1.0. Data Buoy Co-operation Panel Tech. Doc. 4, SIO 95-27, WOCE Rep. 34/95.
Vagle, S., W. G. Large, and D. M. Farmer, 1990: An evaluation of the WOTAN technique of inferring oceanic winds from underwater ambient sound. *J. Atmos. Oceanic Technol.*, **7,** 576–595.
Vakkayil, R., H. C. Graber, and W. G. Large, 1996: Ambient noise measurements with WOTAN during the Surface Wave Dynamics Experiment (SWADE). Tech. Rep. RSMAS 96-004, Rosenstiel School of Marine and Atmospheric Sciences, University of Miami, 66 pp.
Weller, R. A., R. E. Payne, W. G. Large, and W. Zenk, 1983: Wind measurements from an array of oceanographic moorings and from *F/S Meteor* during JASIN 1978. *J. Geophys. Res.*, **88** (C14), 9689–9705.
Wentz, F. J., and D. Smith, 1999: A model function for the ocean-normalized radar cross section at 14.6 GHz derived from NSCAT observations. *J. Geophys. Res.*, **104,** 11 499–11 514.
——, S. Peteherych, and L. A. Thomas, 1984: A model function for ocean radar cross sections at 14.6 GHz. *J. Geophys. Res.*, **89,** 3689–3704.
——, L. A. Mattox, and S. Peteherych, 1986: New algorithms for microwave measurements of ocean winds: Applications to Seasat and the Special Sensor Microwave Imager. *J. Geophys. Res.*, **91,** 2289–2307.
Wikle, C. K., L. M. Berliner, and N. Cressie, 1998: Hierarchical Bayesian space–time models. *J. Environ. Ecol. Stat.*, **5,** 117–154.
——, R. F. Milliff, D. Nychka, and L. M. Berliner, 2001: Spatiotemporal hierarchical Bayesian modeling: Tropical ocean surface winds. *J. Amer. Stat. Assoc.*, **96,** 382–397.